Effects of different correction algorithms on absorption coefficient – A comparison of three optical absorption photometers at a boreal forest site ~~– effects of different correction algorithms~~

Krista Luoma[1], Aki Virkkula[2], Pasi Aalto[1], Katrianne Lehtipalo[1,2], Tuukka Petäjä[1] and Markku Kulmala[1]

[1]Institute for Atmospheric and Earth System Research, University of Helsinki, Helsinki, 00014, Finland
[2]Atmospheric Composition Research, Finnish Meteorological Institute, Helsinki, 00560, Finland

Correspondence to: Krista Luoma (krista.q.luoma@helsinki.fi)

Abstract.

We present a comparison between three absorption photometers that measured ~~the~~ absorption coefficient (σ_{abs}) of ambient aerosol particles in 2012 – 2017 at SMEAR II, a measurement station located in a boreal forest in southern Finland. The comparison included an Aethalometer (AE31), a Multi Angle Absorption Photometer (MAAP), and a Particle Soot Absorption Photometer (PSAP). These optical instruments measured particles collected on a filter, which is a source for systematic errors, since in addition to the particles, also the filter fibers interact with ~~the radiation~~light. To overcome this problem, several algorithms have been suggested to correct ~~the data measured by~~ the AE31 and ~~the~~ PSAP measurements. ~~Our~~ The aim of this study wa~~i~~s to research~~study~~ how the different correction algorithms affected the derived optical properties. We applied the different correction algorithms to the AE31 and PSAP ~~data, and~~data and compared the results against the reference measurements conducted by the MAAP. The comparison between the MAAP and AE31 resulted ~~to~~ in a multiple scattering correction factor (C_{ref}) that is used in ~~the~~ AE31 correction algorithms to compensate for the light scattering by ~~the~~ filter fibers. The C_{ref} varies between different environments~~,~~ and our results are applicable for ~~measurements conducted in~~ a boreal environment. We observed a clear seasonal cycle ~~of~~ in C_{ref}, which was probably due to ~~the~~ variations in aerosol optical properties, such as the backscatter fraction and single-scattering albedo, and also due to ~~the~~ variations in the relative humidity (*RH*). ~~even though the *RH* in the instruments were kept below 40%.~~ The results show~~ed~~ that the filter-based ~~measurement methods~~absorption photometers seem~~ed~~ to be rather sensitive to the *RH* even if the *RH* wa~~i~~s kept below the recommended value of 40%. The instruments correlated well ($R \approx 0.98$) but the slopes of the regression lines varied between the instruments and correction algorithms: compared to the MAAP, the AE31 underestimated the σ_{abs} only slightly (the slopes varied between 0.96~~3~~–1.00~~0.97~~) and the PSAP overestimated the σ_{abs} only a bit (the slopes varied between 1.01~~7~~–1.04 for a recommended filter transmittance > 0.7~~24~~). The instruments and correction algorithms had a notable influence on the absorption Ångström exponent: the median absorption Ångström exponent varied between 0.93 – 1.54 for the different algorithms and instruments.

1 Introduction

Atmospheric aerosol particles have a notable effect on the Earth's radiative balance. The particles affect the Earth's climate directly by scattering and absorbing ~~the~~ radiation from the sun, and indirectly through ~~the~~ aerosol-cloud interactions (Stocker et al., 2013). According to the IPCC report (Stocker et al., 2013), one of the greatest uncertainties in determining the global radiative forcing is related to the atmospheric aerosol particles. Reasons for the large uncertainty are the complex nature of ~~the~~ aerosol-cloud interactions and also the ~~large~~ great spatiotemporal variation of ~~aerosol~~ the particles (Lohmann and Feichter, 2005). Since the number concentration, size distribution, chemical composition and the shape of the particles vary in both space and time, it is challenging to model and estimate the effect that the aerosol particles have on ~~the~~ climate on a~~in~~ global scale (Stocker et al., 2013).

Generally, the direct effect of ~~the~~ aerosol particles on climate is cooling, since most of the particles scatter ~~the light~~radiation from the sun back in to ~~the~~ space (Stocker et al., 2013). However, if particles that are dark ~~in color~~ (i.e., highly absorbing) are located above a ~~light colored~~bright surface (i.e., highly scattering), the particles have a warming effect on ~~the~~ climate. The sign (i.e., negative sign for the cooling effect and positive sign for the warming effect) of the aerosol forcing efficiency depends on the darkness of the particles, which is described by a single scattering albedo (ω), and on the albedo of the ground below the aerosol layer (Haywood and Shine, 1995). To determine the direct effect of ~~the~~ aerosol particles, in addition to the information about the albedo of the surface, we need measurements of aerosol optical properties (AOPs) like scattering, backscattering and absorption coefficients (σ_{sca}, σ_{bsca} and σ_{abs}). The σ_{sca} ~~describes~~ is a measure of~~the ability of~~ ~~the~~light scattering by the particles ~~to scatter the light~~ in all directions, ~~the~~ the σ_{bsca} ~~describes~~is a measure of light scattering ~~the amount of scattering~~ only in the backward direction, and the σ_{abs} ~~describes~~ is a measure of~~the ability of~~ ~~the~~ particulate light~~les to~~ absorp~~b~~tion ~~light~~. All these variables are wavelength dependent, which is why the measurements of AOPs are preferably conducted at multiple wavelengths.

Measuring the σ_{sca} and σ_{bsca} ~~of aerosol particles~~ is rather straightforward and the measurements are typically conducted with an integrating nephelometer. Correction algorithms and coefficients to minimize the~~The~~ error sources and uncertainties of integrating nephelometers ~~measurements~~ are ~~well known~~ systemically used (Anderson and Ogren, 1998; Müller et al., 2011b). However, for the σ_{abs} measurements there are still large uncertainties and the error sources are not as well defined as for the σ_{sca} and σ_{bsca} ~~scattering~~ measurements. The main difference between the σ_{sca} and σ_{abs} measurements is that the σ_{sca} measurements are conducted for particles suspended in air, whereas the σ_{abs} is typically measured by filter-based techniques, where the aerosol particles are ~~first~~ collected on a filter ~~before the measurements~~. The problem with the filter-based measurements is that in addition to the particles, also the filter fibers interact with ~~the~~ radiation and thus~~, which~~ influence~~s~~ the measurements.

One of the issues arising specifically with the optical filter-based measurements is ~~the~~ a multiple scattering of light by the filter fibers. The multiple scattering ~~by the filter fibers~~ is ~~taken into account~~considered by the so-called multiple scattering correction factor (C_{ref}). Even though the C_{ref} should only depend on the properties of the filter ~~properties~~, previous studies have shown that the C_{ref} ~~depends~~ also depends on the particulate matter suspended in the filter (Arnott et al., 2005; Collaud Coen et al., 2010; Weingartner et al., 2003). The C_{ref} has been observed to vary from station to station and therefore, it has been studied in different ~~types of~~ environments. For example, Collaud Coen et al. (2010) studied the C_{ref} at very clean mountain sites, in a maritime site, and in ~~more~~ urban areas; Schmid et al. (2006) did observations in Amazonia; Backman et al. (2017) studied the C_{ref} in Arctic sites; and Kim et al. (2019) ran measurements in a maritime, high altitude, and Arctic sites. Since there is no generally accepted method for deriving the C_{ref} values, the methods between different studies vary, which can also affect the results. In this study, we derived the C_{ref} by comparing two optical filter-based instruments with each other. ~~In our study, one of the aims is to provide a C_{ref} value suitable for a boreal forest site and to study how the C_{ref} varies between different correction algorithms.~~

Another issue with ~~the~~ optical filter-based measurements is related to the nonlinear response of the instruments as the filter is loaded with particles. When the filter is loaded with absorbing particles, the particle loadings ~~cast a so-called shadowing effect, which~~ decreases the response of the instrument. Therefore, the instruments report a lower σ_{abs} for loaded filters compared to pristine filter measurements. Several studies have developed algorithms ~~and determined coefficients~~ to overcome this problem that has been observed with different instruments (Arnott et al., 2005; Bond et al., 1999; Collaud Coen et al., 2010; Li et al., 2020; Müller et al., 2014; Ogren, 2010; Schmid et al., 2006; Weingartner et al., 2003; Virkkula et al., 2005; Virkkula et al., 2007; Virkkula, 2010). In general, after correcting the data for the multiple scattering and loading effects, the absorption instruments agree rather well with the reference measurements (Drinovec et al., 2015; Hyvärinen et al., 2013; Park et al., 2010; Segura et al., 2014). The outcome of the different algorithms, however, varies and they may affect, for example, the wavelength dependency of the σ_{abs} (Backman et al., 2014; Collaud Coen et al., 2010).

~~In our study~~This study has two aims that address the variation in the C_{ref} and the differences between the correction algorithms. ~~, one of the aims~~ The first aim is to provide ~~a~~ C_{ref} values that are suitable for a boreal forest site and to study how the C_{ref} varies ~~between~~for different correction algorithms. The second ~~Another~~ aim ~~of this study~~ is to present how the different correction algorithms of the σ_{abs} affect the measured ~~optical properties of the particle~~and derived AOPs.

The measurements presented in this study, were conducted in 2012 – 2017 at ~~the SMEAR II (~~Station for Measuring Ecosystem-Atmosphere Relations II (SMEAR II; Hari and Kulmala, 2005), which is located in the middle of a boreal forest in southern Finland. During this period, the AOPs at SMEAR II have been measured by several instruments: an integrating nephelometer and three different absorption photometers (AE31, PSAP, and MAAP), which enabled determining the C_{ref} and an extensive comparison between the different instruments and correction algorithms. AOPs at SMEAR II have been extensively discussed

by Virkkula et al. (2011) and Luoma et al. (2019), however, these studies focused on the temporal variation ~~of~~ in the AOPs and they only discussed nephelometer and AE31 data. In this study, we focus on the technical side of the measurements and instrument comparison.

2 Measurements and methods

2.1 The field site

The measurements took place at ~~the~~ SMEAR II ~~station~~ (Station for Measuring Ecosystem-Atmosphere Relations; Hari and Kulmala, 2005). The measurement station locates in Hyytiälä, Southern Finland (61°51'N, 24°17 E). SMEAR II is a rural measurement station and it represents boreal forest environment. The area around the station is mostly forests that ~~, which~~ consists mainly of scots pine trees (Hari et al., 2013). The site is classified as rural and there are no significant~~remarkable~~ sources of pollution nearby. The area is sparsely populated; in the nearby area there are few smaller towns and some scattered settlements. The closest bigger cities are Tampere (220 000 inhabitants) and Jyväskylä (140 000 inhabitants) and they are located 60 and 100 km away from the station.

2.2 Instrument set-up

The measurements of AOPs for PM10 particles were started already on June 2006 with an integrating nephelometer (TSI model 3563) and an Aethalometer (Magee Scientific model AE31). Later on there has also been a Particle Soot Absorption Photometer (PSAP; Radiance Research model 3-λ; Virkkula et al., 2005)~~,~~ and a Multi-Angle Absorption Photometer (MAAP; Thermo model 5012; Petzold and Schönlinner, 2004). ~~and a Cavity Attenuated Phase Shift extinction monitor (CAPS, Aerodyne Research; Kebabian et al., 2007). The CAPS was deployed at the SMEAR II to measure the extinction coefficient (σ_{ext}) of airborne particles. However, the CAPS data was invalidated from this study due to technical issues and therefore the instrument is not discussed in this article.~~

The measurement arrangement of the instruments, which measured the AOPs, is presented in Fig. 1. The schematic figure represents the measurement line from a period when all the instruments mentioned before were measuring in parallel, which was during 2014 – 2015. In the start of the measurement line, a pre-impactor removed all the particles that were larger than 10 µm in aerodynamic diameter (i.e., PM10 passed the pre-impactor). The air flow through another impactor, which removed all the particles larger than 1 µm (i.e., PM1 passed the impactor) was controlled by two valves. The valves changed the direction of the flow in every 10 minutes, so that in a 20-minute measurement cycle the instruments were exposed 10 minutes to the PM10 and then 10 minutes to the PM1. To hinder the effect of changing inlets, the first minutes of the measurements after the inlet switch were omitted. For the absorption instruments the first three minutes and for the integrating nephelometer the first

five minutes were omitted. The sample air was dried with Nafion dryers for the PSAP, AE31, and integrating nephelometer for the whole period and for the MAAP since March 2017. Also, a Cavity Attenuated Phase Shift extinction monitor (CAPS, Aerodyne Research; Kebabian et al., 2007) is marked in Fig. 1, since it was part of the measurement line. However, due to technical issues CAPS data was not applied in this study.

Even though the measurements of AOPs ~~measurements~~ have been conducted at SMEAR II ~~already~~ since 2006, in this study, we consider only data measured after January 2012 until December 2017. This period was selected to have ~~all the three~~at least two absorption instruments running in parallel: the AE31 stopped operating in December 2017, the PSAP operated from January 2012 to March 2016, and the MAAP started operation in June 2013. Also, during this period there were only few changes in the measurement line: in March 2017 the MAAP flow was decreased from 18 lpm to 9 lpm and Nafion dryers were installed in front of MAAP; and in November 2017 one of the two Nafion dryers were removed in front of the n~~N~~ephelometer.

The instruments measured AOPs at different wavelengths: the integrating nephelometer ~~measured the σ_{sca} and σ_{bsca}~~ at three wavelengths (450, 550 and 700 nm); the AE31, the PSAP and the MAAP measured ~~the σ_{abs}~~ at seven (370, 470, 520, 590, 660, 880 and 950 nm), three (467, 530 and 660 nm), and one wavelength (637 nm), respectively. Here, we reported the typically used AE31 and PSAP wavelengths, which are reported in the AE31 manual and by Virkkula et al. (2005), respectively. These reported wavelengths deviate slightly from the ones measured and reported by Müller et al. (2011a) (see their Table 6). For the MAAP, we decided to use the wavelength reported by Müller et al. (2011a) since it more commonly used and it clearly deviated from the wavelength reported by the manual.

The data availability of all the ~~optical~~ instruments~~data~~ for the studied period sets are reported in Fig. S1. Some of the data were missing or invalidated due to instrument malfunctions, too high relative humidity (*RH*), ~~too loaded filter,~~ or due to the absence of the instrument because of workshops or campaigns. If the *RH* exceeded 40% in an instrument, the data was marked as invalid according to recommendations (WMO/GAW, 2016). Before the dryers were installed for the MAAP in March 2017, some of the MAAP data, especially from the summer, ~~had to be~~was invalidated due to too high ~~*humidity*~~*RH*. During the cold season, the indoor temperature at the measurement cottage was higher than outdoors and therefore the *RH* decreased when the sample air was warmed up to the indoor temperature (passive drying). However, ~~during~~ in the summer the *RH* sometimes increased above the accepted limit since the passive drying was not enough due to minimal difference between the indoor and outdoor temperature.

~~The measurement arrangement of the instruments, which measured AOPs, is presented in Fig. 2. The schematic figure represents the measurement line from that time when all the instruments mentioned before were measuring in parallel, which was during 2014 – 2015. In the beginning of the measurement line, a pre-impactor removed all the particles that were larger than 10 µm in aerodynamic diameter from the sample air (i.e., PM10 particles passed the pre-impactor). The air flow trough~~

another impactor, which removed all the particles larger than 1 µm (i.e., PM1 particles passed the impactor) was controlled by two valves. The valves changed the direction of the flow in every 10 minutes, so that in a 20 minutes measurement cycle the instruments measured 10 minutes of the PM10 particles and then 10 minutes of the PM1 particles. The sample air was dried with Nafion dryers for the PSAP, AE31 and integrating nephelometer for the whole period and for the MAAP since March 2017.

2.3 Absorption measurements

As mentioned above, the σ_{abs} of aerosol particles at different wavelengths at SMEAR II was measured with three different instruments: AE31, PSAP and MAAP. Each of these instruments measured the σ_{abs} by filter-based technique, which means that the measurements are conducted for aerosol particles that are collected on a filter. AE31 operated on quartz fiber filter (Pallflex, type Q250F), PSAP on quartz fiber filter (Pall, type E70-2075W), and MAAP on glass fiber filter (Thermo Scientific, type GF 10).

The AE31 and the PSAP have a similar measurement principle (Bond et al., 1999). Before the σ_{abs} can be determined by using different correction algorithms, the instruments measure the attenuation coefficient (σ_{ATN}), which describes is the attenuation of light through the sample collected on the quartz fiber filter. The equation for the σ_{ATN} is derived from the Beer-Lambert-Bouguer law

$$\boldsymbol{\sigma_{ATN}} = \frac{\boldsymbol{A}}{\boldsymbol{Q}\,\boldsymbol{\Delta t}} \ln \frac{\boldsymbol{I_{t-\Delta t}}}{\boldsymbol{I_t}} = \frac{\boldsymbol{A}}{\boldsymbol{Q}} \frac{\boldsymbol{\Delta ATN}}{\boldsymbol{\Delta t}}, \quad (1)$$

where A is the sample area on the filter, Q is the flow through the filter, and Δt is the length of the measurement period. t is the time. $I_{t-\Delta t}$ and I_t are the measured and normalized light intensities through the filter in the beginning of the measurement period ($t - \Delta t$) and in the end of the measurement period (t). The intensities are normalized by comparing them to the intensity measured through a clean reference spot. Normalizing the intensities accounts for possible drifts and changes in the intensities of the LEDs. and ΔATN is the change in attenuation (ATN), which is calculated from the ratio of light intensity through a clean filter (I_0) and through a loaded filter (I_t) as

$$ATN = -\ln\left(\frac{I_t}{I_0}\right) \cdot 100\% \,. \quad (2)$$

In addition to the ATN, the filter loading can also be described by transmittance (Tr)

$$Tr = I_t I_0^{-1}, \quad (3)$$

which can be also presented as a function of ATN (Tr = exp(ATN/100%)). The ATN and Tr represent essentially the same concept, but the way of expressing the change of intensity depends on the instrument used: the ATN is traditionally associated with Aethalometer data and Tr with PSAP data.

In Eq. 1, A is typically a constant value defined by the manufacturer and Q is recorded and reported by the instrument. These values, however, might deviate notably from the real values, and therefore they should be measured. ~~A should be~~ and checked regularly ~~and Q should be monitored continuously and calibrated regularly with a calibrated flow meter~~. If these values differ from the reported ones, the Eq. 1 needs corrections for the A and the Q. At SMEAR II, the sample flow of each instrument was regularly measured with a gillian flow meter and the Q reported by the instruments was corrected to match the gillian measurements. For the PSAP and AE31 we used the A values of 18.1 and 54.8 mm^2 that deviated from the default ones, which were 17.8 and 50.0 mm^2, respectively. The A used by default in the MAAP matched the measured one and therefore it was not corrected.

In ~~the~~ a filter, the light is attenuated because of the absorption and scattering by the particles, but also because of the scattering by the filter fibers, which is called multiple scattering. The scattering by the filter fibers increase the optical path of the light beam through the filter. Therefore, the probability for the light beam to be absorbed by a particle increases. Because of the scattering in the filter medium, the σ_{ATN} is larger than the σ_{abs}. Not only the filter fibers scatter light, but also the embedded aerosol particles scatter light ~~affecting the absorption measurements,~~and cause~~ing the~~ so-called apparent absorption, which is typically ~~taken into account~~considered by subtracting a fraction of scattering from the σ_{ATN}. ~~-~~In addition to the scattering by the fibers and particles, also the increasing number of absorbing particles in the filter affects the instrumental response. The signal response caused by the particulate absorption decreases with increasing filter loading. ~~As the filter gets more loaded with particles, the response of the instrument gradually changes.~~ Absorbing particles induce a so-called ~~"~~shadowing or a loading effect~~", introduced by Weingartner et al. (2003)~~, which decreases the change in the intensity ($I_{t-\Delta t} I_t^{-1}$) as the filter gets more loaded (Weingartner et al., 2003). This means that the ~~response of the~~ instrumental response~~s~~ is no~~t~~-linear with increasing ~~for different~~ filter loading~~s~~. The increasing filter loading has an opposite effect than the scattering of the filter fibers and particles: the absorbing particles collected on the filter decrease the optical path and therefore the reported σ_{ATN} for a loaded filter is lower than for a pristine filter. This non-linearity is ~~taken into account~~considered in the various correction algorithms presented in Sect~~s~~. 2.3.1 and 2.3.2.

The measurement principle of the MAAP is different from th~~e~~at of~~e~~ the AE31 and PSAP (Petzold and Schönlinner, 2004). In addition to the light attenuation measurements, the MAAP also measures the backscattered light from the filter in two different angles. The σ_{abs} is then obtained by using a radiative transfer scheme where the measurements of the backscattering and light attenuation are taken into account (Petzold and Schönlinner, 2004). Because of the backscattering measurements, the MAAP does not suffer as much from the filter artefacts as the Aethalometer and the PSAP ~~and hence it does not need any correction algorithms~~. However, in very polluted environments also the MAAP suffers from a measurement artifact that has to be corrected (Hyvärinen et al., 2013), which at SMEAR II, however, is not the case.

At SMEAR II, the MAAP advanced the filter spot automatically once per day in 24 h intervals. The AE31 also advanced the spot automatically when the *ATN* reached 120 at 370 nm wavelength. The PSAP filters were changed manually and the aim was to be change the filter every second day, but due to weekends and holidays, the filters were sometimes changed only after several days. On average the PSAP filters were changed once per three days.

The reported uncertainties of the MAAP, PSAP and Aethalometer are respectively 12, 13, and as large as 50 % (Arnott et al., 2005; Ogren, 2010; Petzold and Schönlinner, 2004). Müller et al. (2011a) reported that the unit-to-unit variability of the PSAP, ~~Aethalometer~~ AE31 and MAAP were about 8%, 20% and 3%. It must be noted that the unit-to-unit variability is a lot smaller, about 2 % for the new AE33 model (Cuesta-Mosquera et al., 2021). Since the uncertainty and unit-to-unit variability of the MAAP was a lot smaller than for the PSAP and ~~Aethalometer~~ AE31 ~~and because the measurement principle of the MAAP is independent from the PSAP and AE31, since it uses the radiative transfer scheme,~~ we used the MAAP as the reference instrument for measuring σ_{abs}. However, even though the MAAP was used as the reference here, it must be remembered that like all the filter-based photometers, also MAAP suffers from the cross sensitivity to purely scattering aerosol and therefore it does not the best reference instrument (Müller et al., 2011a).

Each of the absorption ~~instrument~~ photometer used in this study have their strengths and weaknesses that determine which instrument is the most useful in different situations. According to the uncertainty and unit-to-unit variability, the MAAP is the most ~~accurate~~ precise instrument for monitoring σ_{abs} and black carbon (BC) concentration, which is typically derived from σ_{abs} measurements. Also, the backscattering measurements from the filter reduce the artefacts caused by the scattering aerosol particles and the filter loading effect making it a more accurate instrument. The MAAP changes the spot in a filter roll automatically and therefore it does not require much assistance from the operator and the instrument can run at a remote station as well. However, it measures the σ_{abs} only at one ~~wavelength~~ wavelength, so it is not possible to do the source apportionment or interpretation on the chemical composition of the absorbing particles, which requires measurements on several wavelengths (see Sect. 3.1 and Eq. 16). The AE31 ~~again~~ has a very wide range of wavelengths, which makes the seven-wavelength Aethalometers, the AE31 and the new model AE33, ~~functional and popular~~ widely used instruments. Like MAAP, the AE31 also operates the filter roll automatically so the instrument does not need that much assistance from the operator. ~~.~~ Unfortunately, the problems with defining the errors caused by the filter material are not that well defined, and the instrument uncertainty and unit-to-unit variability of the AE31 is large ~~(Müller et al., 2011a).~~ ~~(Cuesta-Mosquera et al., 2021)~~ The uncertainty and noise of the PSAP is smaller than that of the AE31, which makes the PSAP a popular especially in areas with low concentrations. Even though the wavelength range is not as ~~good~~ wide as with AE31, the PSAP measures the σ_{abs} at three wavelengths, allowing the use of applications that need the wavelength dependency of σ_{abs}. The ~~problem with~~ PSAP ~~is that the~~ filters ~~have~~ to be changed manually by the user so the instrument is not the best option to deploy at a remote site, but then again the leakage through the filter tape is lesser than for the MAAP and AE31. ~~.~~

2.3.1 AE31 correction algorithms

To determine the σ_{abs} from AE31 measurements, the σ_{ATN} needs to be corrected for the multiple scattering by the filter fibers and for the error caused by the filter loading, and in addition, the scattering of aerosol particles should also be taken into account

$$\boldsymbol{\sigma_{abs}} = \frac{\sigma_{ATN} - a_s \sigma_{sca}}{C_{ref}\, R(ATN)}. \quad (4)$$

The effect of the multiple scattering is corrected with a multiple scattering correction factor (C_{ref}) and it is larger than unity. For the filter loading correction ($R(ATN)$) there are different kind of correction algorithms developed for example by Weingartner et al. (2003), Arnott et al. (2005), Schmid et al. (2006), Virkkula et al. (2007), and Collaud Coen et al. (2010). The R, which equals unity for unloaded filters is less than unity for loaded filters, depends on the filter loading, i.e., ATN defined in Eq. (2). The R can also depend on other factors, such as the ω, and some of the algorithms take also other parameters than ATN into account.

In Eq. (4), the scattering by the aerosol particles is ~~taken into account~~considered by subtracting a fraction (a_s) of the measured scattering (σ_{sca}). However, the algorithms by Weingartner et al. (2003) and Virkkula et al. (2007) ignore the particle scattering subtraction, which makes it possible to apply the corrections algorithms without any σ_{sca} measurements. In Weingartner's algorithm, however, σ_{sca} is ~~taken into account~~considered without the subtraction, as will be shown below. For a comparison, in this study we also present data, which was corrected only for the multiple scattering and not for the filter loading (i.e., the $R = 1$) or scattering by the particles. Below we present the different algorithms determined by Weingartner et al. (2003), Arnott et al. (2005), Virkkula et al. (2007), and Collaud Coen et al. (2010), which were selected to use in this study.

Current recommendation by the WMO and GAW is to assume the $R(ATN)$ unity for the AE31 and to use a C_{ref} value of 3.5, which was determined by a comparison study of different AE31 instruments (WMO/GAW, 2016). Therefore, we also studied "not-corrected" AE31 data for which we did not apply any $R(ATN)$ correction or particulate scattering reduction, but only the multiple scattering correction.

Weingartner et al. (2003) (hereon referred as W2003 and with a subscript WEI) derived an empirical correction algorithm based on laboratory measurements of mixed particles (soot, diesel exhaust, organic coating, ammonium sulfate). ~~Hereon we refer to the algorithm as W2003 and with the subscript WEI.~~ The W2003 correction algorithm interpolates the measurements at higher ATN values, to a point where ATN was 10%. When ATN is lower than 10%, the R is assumed unity. In W2003, the loading correction (R_{WEI}) is

$$R_{WEI}(ATN) = \left(\frac{1}{f} - 1\right)\frac{\ln(ATN) - \ln(10\%)}{\ln(50\%) - \ln(10\%)} + 1. \quad (5)$$

Weingartner et al. (2003) stated that the R ~~is~~ depends on the single-scattering albedo (ω)~~-dependent~~ and they found the following relation for the factor f

$$f = a(1 - \omega) + 1. \quad (6)$$

In Eq. 6, ~~the~~ f is unity (i.e., R is unity), when ~~the~~ ω is unity (i.e., the aerosol is purely scattering). Weingartner et al. (2003) determined that ~~the~~ a in Eq. 6 was 0.87 and 0.85 at 450 and 660 nm, respectively. According to these two values, we interpolated ~~the~~ a for all the seven wavelengths by assuming a linear wavelength dependency. Also, ~~the~~ ω was interpolated to the seven AE31 wavelengths according to the mean σ_{abs}, σ_{sca} and scattering Ångström exponent (α_{sca}) values reported by Luoma et al. (2019; see their article Table 1) for PM10 particles. Using these values, we estimated ~~the~~ f separately for each wavelength and we used those constant values in the correction values. The resulting~~ed~~ a, ω, and f were slightly wavelength dependent and their values are presented in Table 1.

The correction algorithm does not apply the scattering correction by subtraction, so the $a_{s,WEI} = 0$ and therefore parallel scattering measurements are in principle not needed. However, the effect of the particulate scattering is ~~taken into account~~considered in the f since it depends on the ω. If there are no parallel measurements of σ_{sca}, the ω cannot be determined. If there is no estimation on the ω, typically f values for different aerosol types determined by Weingartner et al. (2003) are used. The f values were close to the result Weingartner et al. (2003) acquired from measurements of ambient aerosols in a high alpine site and in a garage ~~(~~f was 1.03 and 1.14 for a "white light" Aethalometer; AE10). For example, Collaud Coen et al. (2010) estimated an intermediate value $f = 1.10$ for Cabauw measurements site based on the study by Weingartner et al. (2003).

Arnott et al. (2005) suggested a correction algorithm, which is hereon we referred as A2005 and with the subscript ARN, based on a well-defined theoretical basis. One big difference to the W2003 is that there is a factor for scattering subtraction. Arnott et al. (2005) determined the scattering subtraction fraction $a_{s,ARN}$ from laboratory measurements using submicron ammonium sulfate particles and the values for different wavelengths are presented in Table 1, however, Arnott et al. (2005) noted that the values of $a_{s,ARN}$ could be different if supermicron aerosol particles are present. The loading correction R_{ARN} was defined as:

$$R_{ARN}\ (ATN) = \left(\sqrt{1 + \frac{\left(\frac{V\Delta t}{A}\right)\sum_{i=1}^{n-1}\sigma_{abs,i}}{\tau_{a,fx}(\lambda)}}\right)^{-1}, \quad (7)$$

where the n indicates the n^{th} measurement after a filter spot change. The correction takes in to account the cumulative σ_{abs} of the particles collected on the filter material. The $\tau_{a,fx}(\lambda)$ is the filter absorption optical depth for the filter fraction x that has particles embedded. ~~The~~To calculate the $\tau_{a,fx}(\lambda)$, we used the same a power law function $\tau_{a,fx}(\lambda) = \tau_{a,fx,521}\cdot(\lambda/521\ nm)^{-0.754} = 0.2338\cdot(\lambda/521\ nm)^{-0.754}$. $\tau_{a,fx}$ as Virkkula et al. (2011) and the resulted values are presented in Table 1. ~~and they were calculated from a power law function $\tau_{a,fx}(\lambda) = \tau_{a,fx,521}\cdot(\lambda/521\ nm)^{-0.754} = 0.2338\cdot(\lambda/521\ nm)^{-0.754}$.~~ The exponent -0.754 was obtained from

a power function fitting to $\tau_{a,fx}$ vs. λ (Table 1 of Arnott et al., 2005), similar as in Virkkula et al. (2011). The $\tau_{a,fx,521} = 0.2338$ is the recommended $\tau_{a,fx}$ value for ambient measurements at 521 nm (Arnott et al., 2005).

Virkkula et al. (2007) proposed a correction algorithm, which is hereon referred as V2007 and with the subscript VIR, that utilizes the so-called compensation parameter (k). The k is determined by comparing the last measurements of a loaded filter to the first measurements conducted with a pristine filter. The compensation parameter is determined for each filter spot (fs) as follows:

$$k_{fs} = \frac{\sigma_{\mathrm{ATN}}(t_{fs+1,\mathrm{first}}) - \sigma_{\mathrm{ATN}}(t_{fs,\mathrm{last}})}{ATN(t_{fs,\mathrm{last}})\sigma_{\mathrm{ATN}}(t_{fs,\mathrm{last}}) - ATN(t_{fs+1,\mathrm{first}})\sigma_{\mathrm{ATN}}(t_{fs+1,\mathrm{first}})}, \quad (8)$$

where the "first" refers to the mean of three first values in a pristine filter (i.e., $fs + 1$) and the "last" refers to the mean of three last values in a loaded filter (i.e., fs). The k is then applied in the loading correction R_{VIR}

$$R_{\mathrm{VIR}}(ATN) = \left(1 + k_{fs}\, ATN\right)^{-1}. \quad (9)$$

This algorithm does not take into account the scattering correction so the $a_{\mathrm{s,VIR}} = 0$.

Collaud Coen et al. (2010) applied this correction to data from several stations in Europe and found that it was highly nonstable and that it leads to large outliers. They correctly stated that the difficulty of applying this correction is due to the natural high variability of σ_{ATN} as a function of time, which is for most of the time greater than the σ_{ATN} decrease induced by filter changes. We therefore calculated the running average compensation parameter for all seven wavelengths in order to minimize these problems. Then we applied this averaged compensation parameter to correct the non-corrected AE31 data. In other words, the AE31 data were not averaged at this stage, just the compensation parameter.

We determined the k as a 14-day running mean (±7 days around the changing time of the filter spot), since without the averaging the k was very noisy (see time series for the non-averaged and averaged k in Fig. S3). Averaging the k was also recommended by Virkkula et al. (2007). On average, the 14-day-periods included about nine data points (i.e., the filter spot changed once per 1.6~~on average about once a~~ days). Virkkula et al. (2015) used a similar approach for AE31 data from Nanjing, China, and calculated 24-hour running averages of the k including on the average six filter spot changes.

Collaud Coen et al. (2010), which is hereon referred as CC2010 and with the subscript COL, correction algorithm was based on the W2003 algorithm but here the reference ATN for the clean filter is 0 % instead of 10 %. They determined the a used in Eq. 6 a bit differently and got a mean value of $a = 0.74$ over different wavelengths and different experiments. The R_{COL} is defined as

$$R_{\mathrm{COL}}(ATN) = \left(\frac{1}{a(1-\bar{\omega}_{0,n})+1} - 1\right) \cdot \frac{ATN}{50\%} + 1. \quad (10)$$

Here the $\bar{\omega}_{0,fs,n}$ stands for the mean $\bar{\omega}_0$, that was calculated for the filter spot from the first measurements to the n^{th} measurement. The $\bar{\omega}_{0,fs,n}$ was determined by using the σ_{ATN} as the first estimate of the σ_{abs}. CC2010 differs from the W2003 also by ~~taking into account~~considering the scattering correction. They suggested two different kind of ways to determine $a_{s,COL}$ and here we present the one that was determined in a manner similar to A2005. The difference to the $a_{s,ARN}$ is that the $a_{s,COL}$ is determined from the ambient scattering measurements so it is not constant. The $a_{s,COL}$ is defined similarly as by Arnott et al. (200~~5~~3) (Eq. 8 in their article), but here they used measured scattering properties instead of constant values determined by laboratory measurements:

$$a_{s,COL} = \bar{\beta}_{sca,n}^{d-1} c\lambda^{-\bar{\alpha}_{sca,n}(d-1)}, \quad (11)$$

where $d = 0.564$ and $c = 0.329 \cdot 10^{-3}$. In Eq. 11 the over lined variables, $\alpha_{sca,n}$ and $\beta_{sca,n}$, stand for average properties of aerosols deposited in the filter i.e., mean values from the beginning of the filter measurements until the n^{th} measurement. The $\alpha_{sca,n}$ is the scattering Ångström exponent (see Sect. 3.1 and Eq. 16) and the β_{sca} is acquired from the power-law fit of the wavelength dependency of σ_{sca}:

$$\sigma_{sca} = \beta_{sca}\lambda^{-\alpha_{sca}}, \quad (12)$$

where the fit is calculated with λ and σ_{sca} in units nm and Mm^{-1} to acquire unitless β.

2.3.2 PSAP correction algorithms

Since the measurement principles of PSAP and AE31 are basically the same, the PSAP data needs similar kind of corrections as the AE31 data (Eq. 2). In this study the PSAP data was corrected with two algorithms: one described by Bond et al. (1999) and later specified by Ogren (2010), which is hereon referred as the B1999; the other determined by Virkkula et al. (2005) and later corrected by Virkkula (2010), which is hereon referred as the V2010. The algorithms of Müller et al. (2014) and Li et al. (2020) were not applied.

The B1999 correction algorithm revisited by Ogren et al., 2010 is given by

$$\sigma_{abs} = f(Tr)\,\sigma_0\,~~0.85~~\frac{\sigma_{PSAP}}{K_2} - a_s\sigma_{sca}\frac{K_1\sigma_{sca}}{K_2}, \quad (13)$$

where ~~the $K_1 = 0.02$ and $K_2 = 1.22$ and~~

$$f\sigma_{Tr}{}_{PSAP} = \left(1.5557 \cdot Tr + 1.0227\frac{\sigma_{ATN}}{1.0796 \cdot Tr + 0.71}\right)^{-1}. \quad (14)$$

In the V2010 correction algorithm, the σ_{PSAP} is determined in an iterative manner. The first estimation of absorption coefficient ($\sigma_{abs,0}$), which is determined by $\sigma_{abs,0} = (k_0 + k_1 \ln(Tr))\sigma_{ATN} - s\sigma_{sca}$, where the k_0 and k_1 are constants presented in Table 1

in Virkkula (2010). The $\sigma_{abs,0}$ is used to calculate the single scattering albedo ω (see Sect. 3.1 and Eq. 17), which is then again used to calculate the σ_{abs} again in an iterative manner, but now with a different kind of an equation

$$\sigma_{abs} = (k_0 + k_1 h(\omega_0) \ln(Tr))\sigma_{ATN} - s\sigma_{sca}, \quad (15)$$

where the $h(\omega_0) = h_0 + h_1 \omega$. The ω is then calculated again with Eq. 17. These two steps are repeated until the change in the σ_{abs} is minor. Here, the iteration was stopped one t~~We agreed the result, when t~~he change was less than 1%. It must be noted that this correction algorithm is different from the V2007 determined for the Aethalometer data.

2.3.3 Differences between the algorithms

The W2003 algorithm only depends on the *ATN*, otherwise it applies constant values and it does not consider the scattering subtraction. The A2005 is not a function of *ATN* but it takes the filter loading into account by summing the σ_{abs} of the accumulated particles on the filter spot. It does not assume a constant for the scattering reduction but determines the fraction from the wavelength dependency of σ_{sca}. The CC2010 algorithm is similar to A2005 in a sense that it also defines its own scattering reduction factor and determines the filter loading correction by taking into account the properties of the particles accumulated in the filter. The V2007 only depends on the difference between the last and first measurements of two filter spots and it assumes no constant coefficients. The B1999 algorithm relies heavily on constants that describe the dependency on the *Tr*, whereas the V2010 algorithm is an iterative process that depends on the ω. Both B1999 and V2010 consider the scattering reduction with a coefficient.

2.4 Scattering measurements

The σ_{sca} data is needed ~~in order to~~to subtract a fraction of particulate scattering from the σ_{ATN} in A2005, CC2010, B1999 and V2010. Measurements of σ_{sca} and σ_{bsca} are also needed in determining the ω and the backscatter fraction (b, see Sect. 3.1 and Eq. 18), which are used to explain the observed variations in the results. The ω is also used in CC2010.

The σ_{sca} and σ_{bsca} were measured with an integrating nephelometer (TSI model 3565, Anderson et al., 1996). The integrating nephelometer measured σ_{sca} and σ_{bsca} at three wavelengths (450, 550 and 700 nm). Due to instrumental restrictions, the nephelometer can only measure σ_{sca} on the range of 7° – 170° and σ_{bsca} on the range of 90° – 170°, and therefore a truncation correction is applied to σ_{sca} and σ_{bsca} measurements (Anderson and Ogren, 1998; Bond et al., 2009). The fractional uncertainty of the integrating nephelometer for PM10 has been reported to be ~~below~~ ± 910 % ~~(Anderson et al., 1996)~~ (Sherman et al., 2015). Since scattering by aerosol particles is depends significantly on their size, the particulate light scattering is sensitive to hygroscopic growth. To prevent this, the integrating nephelometer operated with two Nafion-driers as shown in Fig. 1.

3 Data analysis

All the data were averaged ~~for~~ to 1 h intervals. The PM1 and PM10 measurements were not separated in the data analysis~~, but instead~~ and ~~both~~ the PM1 and PM10 data were averaged together. Since all the ~~the~~ instrument measured ~~in~~ the same sample air~~ize range~~, ~~mixing~~ combining the PM1 and PM10 data caused no ~~difference~~ discrepancies between the instruments. Since this study discusses filter-based absorption photometers and the *ATN* in the filters decreases due to the accumulation of both PM1 and PM10, it would have been difficult to separate the effect of the different size cuts in the data analysis and therefore the data of different size cuts were combined.~~(Luoma et al., 2019)~~

3.1 Intensive properties

The intensive properties of aerosol particles are determined from the measurements of the extensive properties, which in our data are σ_{abs}, σ_{sca}, and σ_{bsca}. In addition to the chemical properties and size distribution, the extensive properties also depend on the number and volume concentration of ~~the~~ particles. The intensive properties, however, are independent of the amount of ~~the~~ particles and they depend only on the properties of the particles, such as the shape of the size distribution, chemical composition and shape of the particles. Therefore, intensive properties are useful parameters as they indirectly indicate the properties of the particle population. The intensive properties used in this article are the Ångström exponent (α), single scattering albedo (ω), and backscatter fraction (b) and they are presented below.

The Ångström exponent, (α) describes the wavelength dependency of the optical properties and it can be calculated for example for σ_{abs} and σ_{sca} to acquire the absorption Ångström exponent (α_{abs}) and scattering Ångström exponent (α_{sca}), respectively. The α is defined by

$$\alpha = -\frac{\ln\frac{\sigma_1}{\sigma_2}}{\ln\frac{\lambda_1}{\lambda_2}}, \quad (16)$$

where the σ_1 and σ_2 are the property for which the α is being calculated at wavelengths λ_1 and λ_2, respectively. The α is typically used to interpolate or extrapolate optical properties to different wavelengths. This is useful for example in cases, when instruments measure optical properties at different wavelengths and the measurements between different instruments need to be compared. The wavelength dependency also gives information about the size distribution, chemical composition, and sources of the particles: α_{sca} depends on the size distribution of the particles and α_{abs} depends on both the chemical composition and size distribution. The α_{abs} is typically used in a set of empirical equations, that approximate the source ~~apportionment models~~ of black carbon (BC) (Sandradewi et al., 2008; Zotter et al., 2017).

~~One commonly used property is t~~The single-scattering albedo (ω), which describes how big fraction of the total light extinction ($\sigma_{ext} = \sigma_{abs} + \sigma_{sca}$) is due to scattering:

$$\omega = \frac{\sigma_{sca}}{\sigma_{sca} + \sigma_{abs}}. \quad (17)$$

The lower ω is, the darker the aerosol particles are, which is typically caused by a higher content of black carbon (BC); ω close to unity indicates that the particles are high in scattering material like sulfates or sea salt. Therefore, ω is a rough indicator of the chemical composition of the particles.

The backscatter fraction (b) describes the fraction of backscattering coefficient (σ_{bsca}; meaning that the light scatters in the backward hemisphere) of the total scattering coefficient (σ_{sca}):

$$b = \frac{\sigma_{bsca}}{\sigma_{sca}}. \quad (18)$$

The b is also size dependent. In molecular size range it is 0.5, which means that the particles scatter light evenly in the forward and in the backward direction. For larger particles the b decreases, so the particles scatter light more in the forward direction. ~~Compared to σ_{sca} the b is less sensitive to bigger particles.~~

3.2 Multiple scattering correction factor

As stated by Weingartner et al. (2003), the C_{ref} should in principle only depend on the instrument and the filter material used. The effect caused by different amounts of particles deposited in the filter material and their optical properties should be taken into account by the empirical filter loading correction functions $R(ATN)$. However, as shown by previous studies, the C_{ref} varies both spatially and temporally (Backman et al., 2017; Collaud Coen et al., 2010) and therefore we determined the C_{ref} also at SMEAR II.

In this study, the multiple scattering correction factor (C_{ref}) was defined for the AE31 measurements by using the σ_{abs} measured by the MAAP as the reference absorption coefficient ($\sigma_{abs,ref}$). To determine the C_{ref}, the σ_{ATN} measured by the AE31 had to be corrected for the artefact caused by the increased filter loading and then the measurements can be compared to the reference absorption ($\sigma_{abs,ref}$) measured by the MAAP

$$\boldsymbol{C_{ref}} = \frac{\boldsymbol{\sigma_{ATN}}}{\boldsymbol{R(ATN)\,\sigma_{abs,ref}}}. \quad (19)$$

The C_{ref} was defined separately for data corrected ~~by~~ using W2003, A2005, V2007, and CC2010 to obtain the C_{WEI}, C_{ARN}, C_{VIR}, and C_{COL} respectively. The C_{ref} was also determined for data, which were not corrected for the filter loading (C_{NC}, where subscript NC stands for "not corrected"). Because the MAAP measures the $\sigma_{abs,ref}$ only on the wavelength 637 nm, the closest AE31 and nephelometer data were first interpolated to the same wavelength. The σ_{ATN}, ~~and~~ ATN, ~~measured by the AE31~~ and ~~the~~ σ_{sca} were interpolated to 637 nm by applying the Ångström exponent explained in Eq. 16. Also, the wavelength dependent constants used in W2003 and A2005 were interpolated to 637 nm. The f used in W2003 at 637 nm was 1.12 and the $a_{s,ARN}$ and $\tau_{a,fx}$ used in A2005 were 0.0681 and 0.2009 at 637 nm, respectively.

In the A2005, cumulative optical properties of the particles collected on the filter were needed, and thus the C_{ARN} was determined by iterating; the C_{ARN} was iterated for each filter spot until the median $\sigma_{abs,ref}$ and $\sigma_{abs,ARN}$ agreed within a 1% limit. Because of the iteration, there is one C_{ARN} value for each filter spot. For other correction algorithms, the C_{ref} value was determined by two methods: 1) C_{ref} was determined as the slope of a linear ~~fit~~regression for ~~to $\sigma_{ATN}(R(ATN))^{-1}$ vs. $\sigma_{abs,ref}$ to acquire the C_{ref} value for the whole data~~ the whole data set (linear fit for a loading corrected σ_{ATN} vs. σ_{ref} -plot; Eq. 19); and by 2) simply using the Eq. 19 to acquire the C_{ref} value for each measurement point separately. In the A2005, the C_{ARN} depends on the wavelength. In this study the C_{ARN} was determined only at the 637 nm. Since we followed a similar procedure as presented by Arnott et al. (2005), a fraction of the σ_{sca} was first subtracted from the σ_{ATN}, before determining the C_{ARN}, which is different to Eq. 19.

4 Results and discussion

4.1 Multiple scattering correction for the AE31

The different C_{ref} values were determined by a linear fit ~~for~~by comparing loading corrected AE31 data ~~vs~~to the~~.~~ reference data from MAAP. Since the C_{ref} is described only by the slope of the fit, the intercept in the y-axis of the fit was forced to be zero. For the linear fit we used all the available parallel data from the AE31 and MAAP. The C_{ref} values were 3.00, 3.14, 2.99, and 2.77 for data corrected by W2003, V2007, CC2010, and for data that was not corrected, respectively. The results and their statistical variability are presented in Table 2. The relatively small standard error (SE) and the range of confidence interval (CI) indicate that the difference between the C_{ref} values were statistically significant. However, for example, the difference between C_{WEI} and C_{COL} was small.

The smallest determined C_{ref} value was the C_{NC}, which was expected. Since the σ_{ATN} decreases for a loaded filter and the filter loading correction was not applied, the C_{NC} had~~s~~ to be smaller than for the corrected data. ~~The C_{NC} was considerably lower than for example the C_{WEI} and C_{COL}, which were about 8% higher than the C_{NC}.~~ Since the values of the C_{WEI} and C_{COL} were almost the same, the result suggested~~s~~ that ~~on average,~~ the loading corrections R_{WEI} and R_{COL} had on average a similar effect~~s~~ on the data. ~~The highest values was~~ere determined for the C_{VIR} ~~and C_{ARN}, which were about 13% higher than C_{NC}~~, which. ~~The C_{ARN} was determined differently (iterative process for each filter spot) than other C_{ref} values, which may partly explain the higher values. The C_{VIR}, however was determined similarly to C_{WEI} and C_{COL}. Th~~ suggests~~e~~ reason for the higher C_{VIR} value is that on average, the value of the R_{VIR} was the lowest ~~than the R_{WEI} or R_{COL}~~ (i.e., the effect of filter loading correction in V2007 was stronger).

Since the C_{ARN} was determined in an iterative manner for each filter spot, the C_{ARN} was calculated as the median of ~~all of~~all the filter spots and the resulted value was 3.13, which is also shown in Table 2. This result is not directly comparable to the

other C_{ref} values that were derived as a linear fit. ~~–~~Also, ~~U~~unlike the other algorithms, the A2005 assumed a wavelength dependent C_{ARN}. Here, we were only able to determine the C_{ref} at one wavelength by comparing the interpolated AE31 data to the MAAP measurements at 637 nm ~~so we could not measure the C_{ARN} at different wavelengths~~. To acquire the C_{ARN} at all the seven wavelengths of the AE31, we used the power law function $C_{ARN}(\lambda) = C_{ARN,637nm}(\lambda/637\ nm)^{0.181} = 3.13 \cdot (\lambda/637\ nm)^{0.181}$, where the exponent 0.181 was obtained from a power function fitting to C_{ref} vs. λ in Table 1 of Arnott et al. (2005), similar to Virkkula et al. (2011). $C_{ARN,637nm} = 3.13$ is the value determined above at $\lambda = 637$ nm. The results of the wavelength dependent C_{ARN} values are presented in Table ~~3~~2.

~~The smallest determined C_{ref} value was C_{NC}, which was expected. Since the σ_{ATN} decreases for a loaded filter and the filter loading correction was not applied, the C_{NC} has to be smaller than for the corrected data. The C_{NC} was considerably lower than for example the C_{WEI} and C_{COL}, which were about 8% higher than the C_{NC}. Since the values of the C_{WEI} and C_{COL} were almost the same, the result suggests that on average, the loading corrections R_{WEI} and R_{COL} had similar effects on the data. The highest values were determined for C_{VIR} and C_{ARN}, which were about 13% higher than C_{NC}. The C_{ARN} was determined differently (iterative process for each filter spot) than other C_{ref} values, which may partly explain the higher values. The C_{VIR}, however was determined similarly to C_{WEI} and C_{COL}. The reason for the higher C_{VIR} value is that on average, the value of the R_{VIR} was lower than the R_{WEI} or R_{COL} (i.e., the effect of filter loading correction in V2007 was stronger).~~

According to Collaud Coen et al. (2010), who studied the C_{ref} of different algorithms for ambient measurements in different ~~kinds of~~ environments, the higher C_{ref} values were typically measured in ~~more~~ polluted areas. Observations in our study support this claim. For example, they determined mean C_{WEI} of 2.81, 2.81, 3.05, and 4.09, at Hohenpeissenberg, Jungfraujoch, Mace Head, and Cabauw, respectively. Segura et al. (2014) obtained a C_{ref} value of 4.22 measured in Granada, Spain at 637 nm for the correction algorithm by Schmid et al. (2006). Compared to their study the C_{ref} values at the SMEAR II were obviously lower than the mean C_{ref} values at the Cabauw and Granada measurement station~~s~~. Cabauw~~, which~~ station is located near populated and industrial areas and the station in Granada is located close to a highway.~~,~~ At SMEAR II, the average C_{ref} values~~and~~ were somewhat higher than in the clean mountain stations in Hohenpeissenberg and Jungfraujoch. The closest values were defined for the Mace Head station, which observes mostly marine air. The C_{ref} values by Collaud Coen et al. (2010) and Segura et al. (2014) were determined similar to our study, so by comparing AE31 measurements against MAAP.

Backman et al. (2017) determined C_f (Backman et al., 2017, used the symbol C_f instead of C_{ref} to mark that the comparison was not conducted with a reference instrument) values for ambient data at several Arctic sites. They also derived the C_f optically by comparing Aethalometer measurements against MAAP, PSAP and CLAP (Continuous Light Absorption Photometer; Ogren et al., 2017). They ran the comparison for Aethalometer data that were not corrected for the filter loading error. The median C_f values at 637 nm were 1.61, 3.12, 3.42, 4.01, and 4.22 measured at Summit, Barrow, Alert, Tiksi, and Pallas, respectively. Backman et al. (2017) did not find any clear explanation for the very low C_f at Summit. At the other sites,

the C_f values were rather high compared to the C_{NC} observed at SMEAR II (C_{NC} = 2.77), which is unexpected if we would assume that the C_{ref} was lower at clean environments, such as Arctic, compared to sites closer to pollution sources.

In laboratory runs, Arnott et al. (2005) determined C_{ref} = 2.076 (at 521 nm) for kerosene soot by comparing AE31 against photoacoustic instrument and Weingartner et al. (2003) observed C_{ref} = 2.14 (averaged over wavelengths) for not-coated soot particles by subtracting scattering from extinction measurements. Compared to the C_{ref} determined in laboratory studies by Weingartner et al. (2003) and Arnott et al. (2005), the ambient measurements in our study yielded higher values. This was also observed by Arnott et al. (2005), who suggested C_{ref} = 3.688 (at 521 nm) for ambient measurements, which is closer to our observations. In addition to not-coated soot, Weingartner et al (2003) determined the C_{ref} for coated particles as well and the resulted C_{ref} was higher, about 3.6. This is also closer to our observations, which is ~~probably~~ explained by the fact that at SMEAR II, the observed soot particles are likely aged and coated since there are no significant local emission sources. In these studies, however, the reference instruments were not filter-based photometers and that can have an effect on the results. ~~coated soot describes better the particles observed at SMEAR II, where the soot particles are likely aged and coated since there are no significant local emission sources.~~

The report 227 by WMO and GAW (World Meteorological Organization and Global Atmosphere Watch) recommends to determine the σ_{abs} from Aethalometer measurements by using C_{ref} value of 3.5 and not applying any filter loading correction or particle scattering reduction in the data. The C_{ref} was determined as an average over several datasets collected from different GAW stations. Comparing this value to the C_{NC}, using the recommended C_{ref} = 3.5 would systematically underestimate the σ_{abs} at SMEAR II by ~~about~~ ~20%. It must be also noted, that due to the lack of $R(ATN)$ correction, the BC concentration or σ_{abs} may differ as much as 50% even if the ~~real~~ true σ_{abs} would stay constant (Arnott et al., 2005). Therefore, in some cases, the data user may want to take the error caused by the filter loading into account and to use different correction algorithms. For example, when studying shorter time periods (e.g., few days of data, which may fit few filter spot changes causing apparent variation in the measured concentration).

There are both studies where constant C_{ref} has been used and studies where wavelength dependent C_{ref} has been used. Others observed no significant dependency for the C_{ref} on the wavelength (Backman et al., 2017; Bernardoni et al., 2021; Collaud Coen et al., 2010; Weingartner et al., 2003; WMO/GAW, 2016) and other studies observed the opposite and showed that the C_{ref} is wavelength dependent (Arnott et al., 2005; Kim et al., 2019; Schmid et al., 2006). These studies suggested that C_{ref} increaseds with wavelength (i.e. filter fibers scattered more light at longer wavelengths). Interestingly, even though the wavelength dependency was not statistically significant~~t is worth pointing out that, also~~ Weingartner et al. (2003) reported that the C_{ref} ~~presented slightly wavelength-dependent C_{ref} values, even though in the literature mainly their average value of 2.14 is cited. Interesting is also, that the wavelength dependency they~~ obtained for internal mixtures of Diesel soot and

ammonium sulfate and coated Palas soot yielded $C_{ref} = 3.9 \cdot (\lambda/660\ nm)^{0.18}$ and $C_{ref} = 3.66 \cdot (\lambda/660\ nm)^{0.23}$, respectively, as can be calculated from their Table 3. The exponents are very close to the value 0.18 obtained from the fittings to the Arnott et al. (2005) Table 1. Kim et al. (2019) found ~~during the Cheju ABC Plume Monsoon EXperiment (CAPMEX)~~ that C_{ref} depended on wavelength even more strongly, a fitting to their Table 2 yield~~sed~~ $C_{ref} = 4.48(\lambda/532nm)^{0.48}$. Because the results between the different studies vary, it is difficult to conclude whether the C_{ref} is wavelength dependent or not. To study the wavelength dependency of C_{ref}, it would be ideal to use a photoacoustic or σ_{ext}-σ_{sca} -methods as the reference measurements, since they are independent from the filter artefacts.~~In these three studies, the absorption standard was a non-filterbased multiwavelength method.~~

Newer model of the Aethalometer, AE33, applies the so-called dual-spot correction so the instrument operators do not need to apply the correction algorithms themselves. However, the value of C_{ref} is an open question for the AE33 also but since its filter material is different from the one used in the AE31, the results of the present study are not applicable to it. The filter material in AE33 is Teflon-coated glass filter tape (Pallflex type T60A20), but also the "old" filter tape (Q250F) has been used with AE33 and the recommended C_{ref} values to use with these filters are 1.57 and 2.14, respectively (Drinovec et al., 2015).

The different C_{ref} values were not only determined as a linear fit that considered ~~averaging over~~ the whole time series. In addition to the results from linear fits, the Table 2 presents the median, mean, and standard deviation of different C_{ref} values that were determined separately for each data point according to Eq. 19. Determining the C_{ref} separately for each data point enabled studying the temporal variation ~~of~~ in C_{ref}; for example, the times series of the different C_{ref} values are presented in Fig. S2~~1~~. The median and mean values differed somewhat from the slopes of the linear fits, which were about 10% lower than the median values. Comparing the median and mean values shows no large difference, meaning that the C_{ref} values were rather normally distributed. The variation ~~of~~ in median C_{ref} values between the different correction algorithms was small compared to the relatively large standard deviation (see Table 2).

The C_{ref}, determined separately for each data point, was not stable over time (see time series presented in Fig. S2~~1~~) and we observed seasonal variation for the C_{ref}, which is presented in Fig. ~~3~~2 for the C_{NC} as an example.~~.~~ The seasonal variation was not observed only for the C_{NC}, but also for the C_{WEI}~~, C_{ARN},~~ and C_{COL}, which is presented in Fig. S3~~2~~. Figure ~~3~~2 shows that the C_{NC} was clearly above the median during the summer and below the median in winter and early spring. The C_{NC} reached its maxima in July and its minima in February. For C_{VIR} and C_{ARN}, ~~T~~the seasonal variation was much less pronounced (Fig. S3). ~~of the C_{VIR} differed from the other algorithms so that the seasonal variation was not as clear. Figure 3 shows that the C_{NC} was clearly above the median during the summer and below the median in winter and early spring. The C_{NC} reached its maxima in July and its minima in February.~~

Since the C_{WEI}, C_{ARN}, and C_{COL} had a similar seasonal variation, it is unlikely that the seasonal variation observed for C_{NC} was caused by the lack of filter loading correction. It is actually rather surprising, that tThere was a seasonal variation for the C_{WEI}, C_{ARN}, and C_{COL} as well and for example, the seasonal variations between the C_{WEI} and C_{COL} were rather similar, even though we applied constant f values in W2003. The algorithm by CC2010 considers the wavelength dependency of scattering and the ω of the accumulated particles. It is rather surprising that taking these parameters, which have a seasonal variation at SMEAR II (Luoma et al., 2019; Virkkula et al., 2011), did not seem to reduce the seasonality of C_{ref}. A2005 and CC2010 took into account the ambient ω, which has a clear seasonal variation at SMEAR II (Luoma et al., 2019; Virkkula et al., 2011), but against the assumptions, this is not seen in the results. For example, the seasonal variations between the C_{WEI} and C_{COL} are surprisingly similar, even though we applied constant f values in W2003 However,

Tthe seasonal variations for in the C_{ARN} and C_{VIR} wereas a little less obvious than for in C_{WEI}, C_{COL}, and C_{NC}, which The lesser seasonal variation for the C_{ARN} might be explained by the subtraction becauseof the scatteringa fraction of the σ_{sca} was subtracted before the loading correction was applied and the C_{ARN} was determined. The fact that the C_{ARN} has less data points than the other the C_{ref} values, might also explain part of the lesser seasonality. For C_{VIR}, tThe lack of seasonal variation for C_{VIR} waiis probably caused by the very strong seasonal variation of in the compensation parameter (k; see Fig. 10a) as will be discussed below in Sect. 4.4. The algorithm by V2007 does not assume any coefficients but depends only on the difference between the last and first measurements of the filter spots. Therefore, it seems to adjust to seasonal changes whereas the other algorithms apply coefficients. According to our results, It seems that the V2007 and A2005 is more dependent onaccounted well the variations in the optical properties of the particles embedded in the filter than the other algorithms are and therefore the seasonal variations in the C_{VIR} and C_{ARN} wereis reduced. The k is discussed more in Sect. 4.4.

The seasonal variations of the C_{ref} values might be explained by the fact that theAs indicated by the seasonal variation, the C_{ref} is was not necessarily a constant value, but it dependsed on the optical properties of the particles, which are embedded in the filter. As stated before, Weingartner et al. (2003) and Arnott et al. (2005) both observed different C_{ref} values for different types of aerosols so that the C_{ref} was lower for "pure" soot (no coating) and higher for coated soot or ambient aerosol particles. This would suggests that the C_{ref} increases with increasing ω. This supports our observations, since at SMEAR II, the ω is the highest in summer and lowest in winter (Luoma et al., 2019; Virkkula et al., 2011). However, Collaud Coen et al. (2010) observed a decreasing trend for C_{ref} with increasing ω when they compared the average conditions at several stations.

The ω, however, is not the only optical property of aerosol particles that had a clear seasonal variation (Luoma et al., 2019; Virkkula et al., 2011). For example, the size dependent b and α_{sca} reached their maxima in summer and minima in winter, which indicatedds that in summer the fraction of smaller particles increased particle size distribution had relatively more weight on smaller particles. Luoma et al. (2019) showed that the seasonal variation of in b and α_{sca} is explained especially by the differences in accumulation mode (particles in the size range of 100 nm – 1 µm) particle concentration and size distribution:

in summer, the volume concentration peaks around 250 nm and in winter around 350 nm. The size distribution affects the penetration depth of the particles as smaller particles penetrate deeper in the filter (Moteki et al., 2010). Scattering particles that penetrate deeper in the filter increase the multiple scattering in the filter, and that could be one explanation for higher C_{ref} values observed in summer.

The differences in the scattering properties of differently sized particles might also explain the observed seasonal variation ~~of~~ in C_{ref}. The correction algorithms only ~~take into account~~consider the amount of scattering, but not the direction of scattering. ~~The s~~Smaller ~~the~~ particles ~~are, the~~ scatter relatively more ~~the particles scatter~~ light in the backward direction, which increase~~sing~~ the optical path of the light ray through the filter (i.e. C_{ref} should increase). Therefore, this effect may cause the observed increase in the multiple scattering correction factor C_{ref} in summer. This could also explain why the C_{VIR} has~~d~~ no seasonal dependency; the compensation parameter seem ed~~s~~ to depend also on the b (see Sect. 4.4) and that would make the V2007 the only algorithm that takes the direction of the particulate scattering into account. Note that the V2007 does not take the b into account directly but it seems to ~~have an effect on~~influence the calculated compensation parameter (see Sect. 4.4).

However, only very weak correlation was found between the C_{NC} and ω (R = 0.17, p-value < 0.05), and C_{NC} and b (R = 0.23, p-value < 0.05), so the ω and b do not necessary explain the observed seasonal variations in the C_{ref} values. For the C_{WEI} and C_{COL}, the results were similar, but for C_{VIR}, the R-values were even lower and even insignificant for ω. ~~re were only weak evidence on the dependency between the C_{ref} and optical properties of the aerosols, which could explain the seasonal variation of the C_{ref}.~~

~~However, w~~We observed slightly higher~~moderate~~ correlation (R = 0.30, p-value < 0.05) between the C_{NC}~~$_{ref}$~~ and relative humidity (*RH*) ~~measured in the MAAP~~, which is presented in Fig. ~~4 for the C_{NC}~~3 (the correlation was similar for C_{WEI}~~, C_{APN}, C_{VIR},~~ and C_{COL}, but ~~weaker, about 0.09, for the C_{VIR} as well~~). Therefore, one possible reason for the observed seasonal variation ~~of~~ in the different C_{ref} values could be caused by changes in the instrumental ~~a technical issue, which is related to the difference in the relative humidity (*RH*)~~ and the *RH* differences between the ~~instruments~~MAAP and AE31. The *RH* presented in Fig. 34 was measured in the MAAP and it varied between 5 – 40% since the periods ~~W~~when the filter of the MAAP was exposed for *RH* equal or larger than 40%~~, the data was~~ were excluded from this study.~~:~~ Because the AE31 was equipped with Nafion-dryers, ~~for the AE31,~~ the *RH* in the AE31 varied less and ~~the *RH*~~ was in the range of 5–20%. ~~When the filter of the MAAP was exposed for RH equal or larger than 40%, the data was excluded from this study.~~

~~Figure 4 shows that the C_{NC} was higher when the sample air was more moist.~~ The *RH* can influence filter-based optical measurements by affecting to the optical properties of the aerosol particles and the filter fibers as well as by affecting the penetration depth of particles in the filter medium. The effect of rate of change in *RH* on the C_{ref} was also studied, but the rate of change in *RH* did not show any correlation between C_{NC}.

~~The optical properties of the filter may change if the filter is exposed to high *RH* conditions. The aerosol particles may take up water even below super saturation and when the liquid particles collide on the filter the moisture is taken up by the filter.~~ Due to the hygroscopic growth, the aerosol particles scatter more light in humid conditions compared to dry conditions.~~T~~ The enhanced scattering induced by higher *RH* could then increase the scattering and optical path in a particle-laden filter medium. However, at SMEAR II, increasing *RH* should have caused a decrease in C_{NC}, since hygroscopic growth would have increased the particulate scattering especially in the reference instrument MAAP. The ~~*RH*~~ hygroscopic growth may also affect the penetration depth of the particles in the filter~~, since the particles grow due to the water uptake~~ (Moteki et al., 2010). When particles are penetrated deeper in the filter, the effect of the multiple scattering is higher increasing the measured σ_{ATN}. Because the *RH* in the MAAP was higher than in the AE31, the particles directed in the AE31 may have penetrated relatively deeper in the filter than the particles directed in the MAAP filter~~. In winter, when the RH was low in both of the instruments the penetration depth would be more similar for each instrument. I~~, in summer, larger difference in the *RH* between the instruments could have ~~then~~ increased the measured C_{ref}. ~~This result shows that even though we have excluded the high *RH* data, the instruments seem to be sensitive to variations in RH even below the recommended 40%.~~ However, the hygroscopic growth should not be significant in *RH* conditions below 40%, which is why the effects related to hygroscopic growth seem unlikely explanations.~~the penetration depth depends also on the filter material, which is different for MAAP and AE31.~~

Also, ~~T~~the optical properties of the filter may change if the filter is exposed to high *RH* conditions. The aerosol particles may take up water even below super saturation and when the liquid particles collide on the filter the moisture is taken up by the filter.

Kanaya et al. (2013) compared the MAAP against Continuous Soot Monitoring System (COSMOS; Miyazaki et al., 2008) and actually observed a slight dependency in the σ_{abs} measured by MAAP so that at low *RH* (< 40%) the σ_{abs} increased with increasing *RH*, which is contrary to our results as we observed that MAAP observed relatively lower σ_{abs} at higher *RH*. However, they also observed opposite behavior at higher *RH* (> 50%). They suggested that the *RH* affected the surface roughness of the filter, which is used in the radiative transfer scheme (Petzold and Schönlinner, 2004), and therefore could have affected the C_{ref}.

Thi~~s~~e results showed~~s~~ that even though we ~~have~~ excluded the high *RH* data, the instruments seemed to be sensitive to variations in *RH* even below the recommended 40%. However, the reason for the sensitivity remains unclear and would require more research and measurements and therefore ~~F~~further analysis is omitted ~~here~~from the scope of this article.

4.2 Performance of the correction algorithms

In this section, we included data from June 2013 to February 2016 to have all the three absorption instruments running in parallel to prevent any differences caused by different periods.

Since the σ_{abs} derived from AE31 measurements used the C_{ref} values determined here, the σ_{abs} measurements of AE31 and MAAP were expected to agree well, which is shown in Fig. ~~5~~4. The AE31 data in Fig. ~~5~~4 was produced by applying the C_{ref} values determined from the linear fits (Table 2 column "fit"). The correlation coefficients and slopes of the linear fits presented in Fig. ~~5~~4 were close to unity. T~~However, all t~~he AE31 correction schemes underestimat~~ed~~ed the σ_{abs} only slightly ~~a bit~~ and the slopes varied from 0.9~~63~~ to 1.00~~0.97~~. ~~-~~The AE31 data corrected with the A2005 and CC2010 underestimated the σ_{abs} the most (slopes of the linear fits were 0.97 and 0.96, respectively~~3~~). The reduction of particulate scattering in CC2010 after applying the multiple scattering correction (i.e., C_{ref}) could explain~~s~~ the slight underestimation in CC2010 derived data. For the underestimation in A2005 derived data, the reason is probably the different way of determining the C_{ARN} compared to other C_{ref} values. The iterative manner of determining the C_{ARN} separately for each filter spot and then taking the median from these values was not as successful as the linear fit ~~–~~-method, which was used for the other algorithms. However, the underestimation for A2005 and CC2010 are only minor.

Surprisingly, the not~~-~~-corrected (NC) AE31 data (Fig. ~~4~~5e) did not seem to have a significant difference in correlation coefficient compared to, for example, ~~to~~ the data corrected with W2003 or CC2010 (Figs. ~~5~~4a and d, respectively). However, the relation between the $\sigma_{abs,NC}$ and σ_{ref} ~~seemed to~~ depend~~ed~~ more on the *ATN* than for any filter loading corrected data, which is shown by the color coding (*ATN*) of the data points and in Table 3, which presents~~,~~ the slopes of the linear fits and R^2 values for different *ATN* intervals. If only data from highly loaded filter (*ATN* > 60 at 660 nm) were taken into account, the slopes of the linear fits were 0.9~~7~~2, 1.0~~6~~0, 0.9~~9~~6, 0.9~~5~~0, and 0.~~93~~88 for W2003, A2005, V2007, CC2010, and ~~not corrected (~~NC~~)~~, respectively. The smallest decrease in the slope with increasing *ATN* determined for the loaded filter was observed for data that was corrected by V2007. Interestingly, the slopes for the loaded filter ~~actually increased~~increased for data that was corrected by A2005~~, meaning that the R_{ARN} had a relatively big effect with increasing *ATN*~~. This different behavior is probably caused by the fact that the A2005 algorithm did not consider the loading through *ATN* but applied a cumulative σ_{abs}, which apparently at SMEAR II seemed to overestimate the loading and loading correction, thus leading to an increasing slope with the *ATN*. The biggest decrease in the slope determined for a highly loaded filter was observed for the ~~not corrected~~NC data, as expected.

~~This observation underlines the need for filter loading correction if one studies shorter time periods. For longer time periods (e.g., trend analysis or studies of seasonal variation) the effect of the *ATN* smooths out, but for shorter time periods (e.g., case studies) the changing *ATN* can have a notable effect on the results if no filter loading correction is applied.~~

According to the R^2 values presented in Table 3, the precision of the AE31 decreased with increasing *ATN*. For example, the data corrected with the A2005 algorithm, the R^2 decreased from 0.96 for a clean filter (*ATN* < 20) to 0.90 for loaded filter (*ATN* > 60). However, the decrease in R^2 was quite minor. Miyakawa et al. (2020) observed also rather high R^2 values between Aethalometer (model AE51) and a reference instrument (single particle soot photometer and COSMOS) when the *ATN* was below 70, but when the *ATN* exceeded 70, the R^2 decreased more rapidly. Unlike for the AE31, the loading on the filter did not seem to affect to the precision of the PSAP at all as the R^2 values did not decrease with increasing loading.

As presented in Table 3, the linear fits for the AE31 and PSAP data against the reference did not have an intercept of zero. This could be caused by the scattering artifact and the fact that the correction algorithms failed to take the scattering artefact partly into account. The intercept is the smallest for the B1999-corrected PSAP data and the largest to AE31 data. A fraction of σ_{sca} is subtracted in the AE31 algorithms by A2005 and CC2010. However, the data corrected with these algorithms still have a higher or similar intercept as with the not-corrected data and the data corrected by the W2003 and V2007 algorithms. Considering the intercept, the V2007-corrected data performs the best in the AE31 vs. MAAP comparison, which is slightly surprising, since it does not take the scattering subtraction into account. For the V2010-corrected PSAP data, the intercept is negative suggesting that the V2010 algorithm overestimates the apparent absorption by scattering particles.

The comparison between the MAAP and the PSAP is presented in Figs. 6a and b and in Table 3 for both the correction schemes B1999 and V2010, respectively. F~~The f~~igure 6b shows that V2010 overestimated the σ_{abs} especially when the loading was high (*Tr* was low~~).~~ and the ~~For the whole data set the slope of the~~ linear regression was 1.254. Also the B1999 overestimated the σ_{abs} slightly, but in general it performed better in comparison with MAAP and the slope was 1.07 (Fig. 6a). ~~If we calculate the linear regression for clean filter situations, when the *Tr* > 0.7 (at 660 nm), the slope of the linear fit is 1.01. For more loaded filter, with a limit of *Tr* > 0.5 (at 660 nm), the slope is 1.08.~~ The linear fits in Figs. 6a and b include all the data, but Table 3 presents the slopes of the linear fits for data with different *Tr* limits. It is actually recommended to use PSAP data with *Tr* > 0.7 and if only this data is taken into account, especially the data corrected with the V2010 algorithm performs much better and has a slope of 1.01, but also the slope for the data derived with the B1999 algorithm yields a smaller slope of 1.04.

If all the data were included in the comparison, as in Figs. 6a and b, the overestimation of σ_{abs} would suggest deriving the C_{ref} values also for the PSAP data. Here, we did not derive the C_{ref} values for the PSAP since they are not typically used in a similar way as for deriving the σ_{abs} from the AE31 measurements. In general, the multiple scattering does not cause such a big artefact in filter material typically used in PSAP compared to the thicker AE31 filters. However, if we considered only the data below *Tr* < 0.7

the PSAP and MAAP agree well for both correction algorithms. This result then suggests that there is no need for deriving a new C_{ref} for PSAP. Svensson et al. (2019) studied the multiple scattering in quartz filters and they derived the equations that

can be used in determining the C_{ref} value for PSAP. Differently to AE31 correction algorithms, the C_{ref} used in PSAP algorithms is included in the coefficients of Eqs. 13 – 15 and therefore determining the C_{ref} for PSAP is not as straightforward.

The differences between these two correction algorithms are studied in more detail in Fig. 6c, which shows how the algorithms perform with different *Tr* and ω values. ~~The figure shows that~~As discussed before, the V2010 produces notably higher σ_{abs} values when the filter is highly loaded (*Tr* < 0.5). However, ~~T~~the difference between the algorithms does not only depend on the *Tr* but ~~depends~~ also on the ω so that at high ω and *Tr*, $\sigma_{abs,PSAP,VIR}/\sigma_{abs,PSAP,BON}$ < 1 and when ω decreases the $\sigma_{abs,PSAP,VIR}/\sigma_{abs,PSAP,BON}$ ratio grows. The reason is that the V2010 algorithm is a function of ω.

The dependency of the σ_{abs} on the *ATN* and *Tr* is presented in supplementary material (Figs. S2 and S3). On average, the decrease in the σ_{abs}, which was not corrected for the filter loading ($\sigma_{abs,NC}$ and $\sigma_{abs,PSAP,ATN}$), with the increasing *ATN* and decreasing *Tr* was not clear. This effect is better seen in the results presented in Table 3. However, Fig. S3 shows that especially for the PSAP, the use of correction algorithms decreased the variation, which is a strong recommendation for using the correction algorithms. This is also seen in the AE31 data, but the effect was less notable (Fig. S2).

Because it is impossible to separate the effect of different size cuts from a loaded filter, here the PM1 and PM10 measurements were combined and averaged together. In general, PM1 accounted for about 90% of the PM10 σ_{abs}; for the σ_{sca} the fraction of PM1 was about 75% (Luoma et al., 2019). Because absorbing particles, which is considered to consist mostly of black carbon, are typically in the fine mode (diameter < 1 µm), the σ_{abs} is not expected to deviate much between the different size cuts. However, the differing size cuts, which causes more deviation in the σ_{sca}, could have affected the σ_{abs} measurements since the particulate scattering causes apparent absorption and affect the multiple scattering in the filter. For example, the coarse particles (diameter > 1 µm) do not penetrate as deep in the filter as the fine mode particles, which could possibly influence on the C_{ref} values. In an ideal situation the PM1 and PM10 absorption would have been measured by separate instruments.

Our observations underline the need for filter loading correction, especially if one studies shorter time periods. For longer time periods (e.g., trend analysis or studies of seasonal variation), the effect of the *ATN* on the variation smooths out, but for shorter time periods (e.g., case studies) the changing *ATN* can have a notable effect on the results if no filter loading correction is applied. However, not correcting for the filter loading effect, the precision of the instrument and the σ_{abs} or *BC* concentration on average are reduced, which is why applying a filter loading correction on filter-based photometers is always recommended.

4.3 Absorption Ångström exponent for different correction algorithms

The effect of the correction algorithms on α_{abs} were studied and the average α_{abs} for different correction algorithms of the AE31 and PSAP are presented in Fig. 7. This figure includes only parallel data from both AE31 and PSAP in order to avoid any differences caused by different time periods. For a comparison, the α_{abs} was also determined for the "raw" PSAP data that was not corrected by any algorithms (i.e., σ_{ATN}, see Eq. 1). To have comparable α_{abs} from the different instruments, Fig. 7 included only overlapping AE31 and PSAP data from 2011 – 2015. Since the PSAP operates at three wavelengths (467, 530, and 660 nm), we determined the AE31-related α_{abs} in Fig. 7 by using only the wavelengths 470, 520, 590, and 660 nm of the AE31. The rest of the AE31 wavelengths were omitted from this comparison to minimize the effect of different wavelength ranges have on α_{abs} (for example, see Luoma et al. (2019) Table 1). The α_{abs} was determined as ~~-1×slope of~~ a linear fit over all the selected wavelengths according to Eq. (16)~~to log(σ_{abs}) vs. log(λ) over the selected wavelengths~~. Since Luoma et al. (2019) did not observe a big difference between the PM1 and PM10 α_{abs}, we included both measurements in this comparison.

According to Fig. 7, the median values of α_{abs} varied notably between the different instruments and correction algorithms: the lowest median value of α_{abs} was 0.9385 and it was measured by AE31 and corrected by the CC2010; and the highest median value of α_{abs} was 1.5448 and it was measured by PSAP and corrected by the V2010. The difference between the highest and lowest median values of α_{abs} was about 1.7-fold. The correction algorithms were applied to each wavelength separately and therefore the correction algorithms affected the wavelength dependency of the derived σ_{abs}. The scattering and loading corrections are different for each wavelength because for example the σ_{sca}, ω, *ATN*, and *Tr*, which are used in the algorithms, are wavelength dependent.

For the AE31, we studied the same five correction algorithms as in Sect. 4.1. The lowest median α_{abs} values were ~~observed for~~observed for the not corrected data ($\alpha_{abs,AE,NC}$) and for data that were corrected with the CC2010 and W2003 algorithms ($\alpha_{abs,AE,COL}$ and $\alpha_{abs,AE,WEI}$). The median α_{abs} values for the data corrected with A2005 and 2007 algorithms ($\alpha_{abs,AE,ARN}$ and $\alpha_{abs,AE,VIR}$) were higher, 1.20 and 1.19, respectively.

~~Since we did not have reference measurements on several wavelengths, it is impossible to say which one of the correction algorithms yielded the most truthful value for the α_{abs}. This could be done with several MAAPs operating at different wavelengths or by measuring the particles suspended in the air by photoacoustic method~~ (Bernardoni et al., 2021; Kim et al., 2019)~~. Saturno et al. (2017)~~

The A2005 was the only algorithm that assumed a wavelength dependent C_{ref}. Since the C_{ARN} increased with wavelength (i.e., bigger correction due to multiple scattering at higher wavelengths), taking the wavelength dependency of the C_{ref} into account increases the $\alpha_{abs,AE,ARN}$ compared to other algorithms. The correction factor of the V2007 algorithm depended on the difference between the *ATN* of loaded and clean filter spots. Most of the time *ATN* increased faster at short wavelengths than at long

wavelengths, so the difference between the *ATN* of the loaded and clean filter spots was higher than for longer wavelengths. Therefore, the filter loading correction was bigger for shorter wavelengths and after the correction the difference between the σ_{abs} at different wavelengths increased, increasing the α_{abs} as well.

For the PSAP data, the α_{abs} were generally a bit higher compared to the AE31 derived α_{abs}. The lowest PSAP derived median value for $\alpha_{abs\ PSAP,NC}$ was 1.01, which resulted from data that was not corrected by any algorithm. B1999 resulted for median $\alpha_{abs,PSAP,BON}$ value of 1.04, and the V2010 produced the overall the highest $\alpha_{abs,PSAP,VIR}$, which was 1.48. Similar order of the average α_{abs} from different algorithms was observed by Backman et al. (2014) at an urban station in Elandsfontein, South Africa. For a dataset measured off the east coast of the United States on a research ship, Backman et al. (2014) reported also the highest α_{abs} for the V2010. These results are consistent with each other. The explanation is that in V2010 all constants are wavelength dependent, contrary to the B1999.

The differences between the correction algorithms could possible be decreased by adding or reducing the wavelength dependency of the used constant values. Since we did not have reference measurements at several wavelengths, it is impossible to say which one of the correction algorithms yielded the most truthful value for the α_{abs}. This could be done with several MAAPs operating at different wavelengths, by measuring the particles suspended in the air by photoacoustic method (Kim et al., 2019), by a polar photometer (Bernardoni et al., 2021), or by a Multi-Wavelength Absorption Analyzer (MWAA; Massabò et al, 2013). According to the comparison between AE31 and MWAA by Saturno et al. (2017), the best agreement for the α_{abs} was achieved with uncorrected AE31 data and also the AE31 data corrected by CC2010 agreed well with the reference measurements.

We also studied if the α_{abs} values were affected as the filter got more loaded with particles. Figure 8 presents the α_{abs} derived from AE31 data corrected with different algorithms as a function of *ATN* and Fig. 9 presents the α_{abs} derived from PSAP data as a function of *Tr*. The α_{abs} derived from corrected PSAP data (Fig. 9a and b) did not seem to depend on loading at $Tr > 0.4$ but for higher filter loadings the α_{abs} ~~grow~~ still increased with decreasing *Tr* with both B1999 and V2010 corrections. ~~As a~~In comparison, for the not corrected PSAP data (i.e., σ_{ATN}), the α_{abs} decreased with increasing *Tr* (Fig. 9c). The α_{abs} derived from the AE31 data was also studied; the $\alpha_{abs,AE,WEI}$, $\alpha_{abs,AE,ARN}$, $\alpha_{abs,AE,COL}$, and $\alpha_{abs,AE,NC}$ clearly decreased with increasing *ATN*. If the *ATN* increased from 5 to 70, the decreases in $\alpha_{abs,\ AE,WEI}$, $\alpha_{abs,AE,ARN}$, $\alpha_{abs,\ AE,COL}$, and $\alpha_{abs,\ AE,NC}$ were rather linear and the decreases were around -22, -23, -33, and -27%, respectively.

The $\alpha_{abs,AE,VIR}$, derived from data corrected with V2007, did not seem to depend on the *ATN*, if not taking into account very high filter loadings (*ATN* at 660 nm > 70; on average the filter changed when the *ATN* at 660 nm ≈ 90). In V2007, the *k* was determined for each wavelength separately. ~~In the next chapter, we show that t~~The *k* is ~~typically largest~~often larger for the shorter wavelengths, which means that the nonlinearity caused by the increased filter loading is relatively stronger at the shorter

wavelengths (Drinovec et al., 2017; Virkkula et al., 2007; Virkkula et al., 2015), which was also observed by this study (discussed in the next chapter). ~~When this is not taken into account~~According to these results, the other algorithms but V2007 do not seem to account enough the wavelength dependency of the *R(ATN)* ~~α_{abs} decreases with the increasing *ATN*, which is seen with the other algorithms~~.

4.4 Variations ~~of~~ in the compensation parameter

The variation ~~of~~ in k at SMEAR II has already been studied by Virkkula et al. (2007) who used AE31 data from December 2004 to September 2006. During this period, the AE31 was operating without any cut-off and there were no scattering measurements available, and this period was not included in our study. Here, we repeated the analysis for a longer time series and included the σ_{sca} measurements, so we could also determine the b and ω.

The average values of the k are presented in Table 4. The mean values of the k varied from $4.6 \cdot 10^{-3}$ at 370 nm to $2.0 \cdot 10^{-3}$ at 950 nm. The wavelength dependency of k is described by a_k, which is the slope of a linear fit of the k over different wavelengths ($k_\lambda = a_k\lambda + k_0$, see example in Fig. 10b). Negative a_k means that on average the filter loading correction was greater at shorter wavelengths. The light attenuation is stronger at shorter wavelengths due to higher absorption and scattering by the particles and therefore the shorter wavelengths are prone to bigger error caused by the filter loading. At longer wavelengths, the standard deviation of the k was higher, meaning that the k was more sensitive to the particle properties at longer wavelengths. The same observation was noted by Virkkula et al. (2015) as well.

At SMEAR II, we observed that the k and the a_k had a very strong seasonal variation so that the k and a_k were the lowest in summer, which was also noted by Virkkula et al. (2007). The seasonal variation was observed at all wavelengths, but the variation was more pronounced at longer wavelengths. The seasonally averaged k and a_k are presented in Table 4 and an example of the seasonal variation ~~of~~ in k at 880 nm is presented in Fig. 10a. Similar seasonal pattern for the k were also observed by Virkkula et al. (2007), Wang et al. (2011), and Song et al. (2013). In summer, the mean k values at the longer wavelengths (660–950 nm) were ~~actually negative~~negative, meaning that without the correction, the AE31 would actually overestimate the σ_{abs} at longer wavelengths.

Previous studies (e.g., Virkkula et al., 2007; Wang et al., 2011; and Song et al., 2013) suggested that the seasonal variation in k could be due to variations in ω, so that lower ω induced higher k. This ~~correlation~~ behaviour is observed at SMEAR II as shown in Figs. 10a and d; the ω peaks in summer as the k has its minima and the correlation coefficient between the ω and k is -0.47. The variation ~~of~~ in ω also explains the observed negative k values. Virkkula et al. (2007) stated that the negative values are associated with the response of the Aethalometer to scattering aerosols as the negative k are observed when the ω is high. The effect of ω was taken into account for example in the AE31 correction algorithms suggested by Weingartner et al.

(2003), Arnott et al. (2007), and Collaud Coen et al. (2010). Virkkula et al. (2015) presented a theoretical explanation to the ω dependency of *k*, which our analysis supports.

Also, the effect caused by the sizes of the particles has been suggested. The sizes of the particle ~~size~~s affects their scattering properties ~~of the particles~~ and also ~~an effect~~ on their penetration depth in the filter that again ~~, which~~ could affect the *k*. The size distribution of the particle population is described by the *b* so that higher *b* indicates smaller particles. Müller et al. (2014), for example, showed that the effect of asymmetry parameter, which is a function of *b* (Andrews et al., 2006), had an effect on the PSAP data.

The dependency of *k* on both *b* and *ω* was investigated more closely by Virkkula et al. (2015) at SORPES, an urban station located in Nanjing, China. The study showed positive correlation between *k* and *b*, and negative correlation between *k* and *ω*. At SMEAR II, we also observed negative correlation between *k* and *ω* (Fig. 10c). However, contrary to the results by Virkkula et al. (2015), we observed negative correlation between *k* and *b* (Fig. 10d). Virkkula et al. (2015) discussed ~~about the~~ difficulties to show whether the *b* or the *ω* was the dominant property in determining the *k*. At SMEAR II, the *ω* varies in a wider range compared to the observations at SORPES, which could explain some of the observed differences. The mean and standard deviation of *ω* at SMEAR II were 0.87 ± 0.07 (at 550 nm; Luoma et al., 2019) and at SORPES 0.93 ± 0.03 (at 520 nm; Shen et al., 2018). However, a clear reason for the negative correlation between the *k* and *b* at SMEAR II was not found.

5 Summary and conclusions

In this study, we presented a comparison of three different absorption photometers (AE31, PSAP, and MAAP), which measured ambient air at SMEAR II, a rural station located in middle of a boreal forest in southern Finland. We also compared different correction algorithms that are used in determining the absorption coefficient (σ_{abs}) from the raw absorption photometer data. We studied how the algorithms affected the derived parameters and determined multiple scattering correction factor (C_{ref}) applicable at SMEAR II.

To get more reliable AE31 measurements, the AE31 data were compared against the MAAP data to acquire the C_{ref} that is used in the processing of the AE31 data. Previous studies observed that the C_{ref} varied between different types of environments and stations and here it was determined for the SMEAR II station, which represents the atmospheric conditions in a boreal forest. The resulted C_{ref} values were 3.00, 3.13, 3.14, and 2.99 for the algorithms suggested by Weingartner et al. (2003), Arnott et al. (2005), Virkkula et al. (2007), and Collaud Coen et al. (2010), respectively. ~~Previous studies observed that the C_{ref} varied between different types of environments and stations and here it was determined for the SMEAR II station, which represents the atmospheric conditions in a boreal forest.~~ The C_{ref} determined at the SMEAR II can be applied to other boreal forest sites as well and~~.~~ ~~E~~even though the AE31 is ~~the~~ an older model and no longer in production, the results can be used in post-

processing older data sets or at sites that still operate the older AE31. ~~Newer model of the Aethalometer, AE33, applies the so-called dual-spot correction so the instrument operators do not need to apply the correction algorithms themselves. However, the value of C_{ref} is an open question for the AE33 also but since its filter material is different from the one used in the AE31, the results of the present study are not applicable to it.~~

We ~~observed~~ also observed a clear seasonal cycle associated with C_{ref}, which was probably due to the variations in the optical properties of the aerosol particles, such as the b and ω. We also observed some correlation between the C_{ref} and RH even though the RH in the instruments were kept below 40%. These results show that the filter measurement methods seem to be rather sensitive to the RH even if the RH is below the recommended value of 40%.

The results obtained for data corrected with the algorithm by Virkkula et al. (2007) were in many ways different from those obtained by Collaud Coen et al. (2010) who applied the Virkkula et al. (2007) correction to data from several stations in Europe. They found that the compensation parameter (k) used in the algorithm was highly nonstable and that it led to large outliers. They correctly stated that the difficulty of applying this correction is due to the natural high variability of σ_{ATN} as a function of time, which is for most of the time greater than the σ_{ATN} decrease induced by filter changes. We therefore calculated 14-day running average compensation parameters (±7 days around each filter spot) in order to minimize these problems. The approach was obviously successful. It can be recommended that users of this method calculate running averages of k. The suitable period for the running average at each site depends on the rate of change in the ATN, which determines how often the filter spots are changed. According to this study and to the study by Virkkula et al. (2015) time period that includes about 6 – 9 filter spot changes on average seems to yield good results. At SMEAR II, a relatively clean site, this period was 14 days and at SOPRES, a rather polluted site, the period was 24 hours. ~~However, no exact time span can be given, it depends on the concentration level of the measurement site – at a clean site like SMEAR II 14 days was sufficient and in the polluted Nanjing 24 hours.~~

The results showed a great variation between the α_{abs} derived from differently corrected σ_{abs} data and at SMEAR II the median α_{abs} for different algorithms varied in the range of 0.93 – 1.54. We also observed that most of the correction methods did not prevent the change in the wavelength dependency as the filter got more loaded and therefore the α_{abs} decreased notably with increasing attenuation (ATN). The correction algorithm by Virkkula et al., (2007) was the only AE31 correction algorithm, which produced a stable α_{abs} for the increasing filter loading. For example, the α_{abs} derived from Aethalometer measurements is often used to describe the chemical properties of the particles and to describe the source of black carbon. Not taking the used correction algorithm and the effect of increasing filter loading into account, could lead to wrong interpretation of the results. According to our results, applying the Virkkula et al. (2007) correction algorithm could help solving if the changes in α_{abs} were due to real variation or due to increased filter loading.

In general, at SMEAR II, the effect of the filter loading on average did not seem to cause major difference in the measured σ_{abs}. However, a strong effect of increased filter loading was seen in the derived parameter α_{abs}, which encourages to apply a filter loading correction to filter-based absorption data. Even though on average, the σ_{abs} did not seem to be greatly affected by the ~~the results showed that applying a filter loading correction to AE31 data clearly reduces the effect of increasing~~ filter attenuation (*ATN*), the filter loading effect can have a great effect when studying shorter periods and, for example, different seasons, which also justifies ~~and therefore~~ applying a correction to the data. ~~is especially important, if the data is studied for shorter periods.~~ According to our study the correction algorithms by Virkkula et al. (2007) and Arnott et al., (2005) performed the best in taking the seasonal variations of the aerosol particles into account. Also, the algorithm by Virkkula et al. (2007) produced the most stable α_{abs} that did not depend on the *ATN*, which was not the case for the other algorithms.

When applying a correction algorithm to AE31 data, it is important to report which algorithm, C_{ref} values and other coefficients were used to acquire the final data product, since the algorithms can have a notable effect on the results, especially on the ~~absorption Ångström exponent~~ α_{abs}. Our results showed that in general, it is a good practice to perform the analysis of AE31 data by using few different correction algorithms, to see if the results vary notably for different algorithms.

Author contributions

KL performed the data analysis and wrote the paper together with AV. PA and AV have set up the aerosol optical measurements at SMEAR II. All authors reviewed and commented on the paper.

Acknowledgements

We thank SMEAR II staff for taking care that all the measurements were running.

Financial support

This research has been supported by the European Union's Horizon 2020 research and innovation program via projects ACTRIS-2 (grant no. 654109) and iCUPE (grant no. 689443). Additional financial support was received through the Academy of Finland (Center of Excellence in Atmospheric Sciences) under the projects PROFI-3 (decision no. 311932), NANOBIOMASS (decision no. 307537). This research was also supported by Academy of Finland via project NABCEA (grant no. 29664) and by Business Finland via project BC Footprint (grant no. 49402-201040). Financial support of University of Helsinki to ACTRIS-FI is gratefully acknowledged.

References

Anderson, T., Covert, D., Marshall, S., Laucks, M., Charlson, R., Waggoner, A., Ogren, J., Caldow, R., Holm, R., Quant, F., Sem, G., Wiedensohler, A., Ahlquist, N., and Bates, T.: Performance characteristics of a high-sensitivity, three-wavelength, total scatter/backscatter nephelometer, J. Atmos. Ocean Tech., 13, 967-986, 1996.

Anderson, T., and Ogren, J. A.: Determining aerosol radiative properties using the TSI 3563 integrating nephelometer, Aerosol Sci. Technol., 29, 57-69, 10.1080/02786829808965551, 1998.

Andrews, E., Sheridan, P., Fiebig, M., McComiskey, A., Ogren, J., Arnott, P., Covert, D., Elleman, R., Gasparini, R., Collins, D., Jonsson, H., Schmid, B., and Wang, J.: Comparison of methods for deriving aerosol asymmetry parameter, J. Geophys. Res. Atmos., 111, 10.1029/2004JD005734, 2006.

Arnott, W. P., Hamasha, K., Moosmüller, H., Sheridan, P. J., and Ogren, J. A.: Towards aerosol light-absorption measurements with a 7-wavelength Aethalometer: Evaluation with a photoacoustic instrument and 3-wavelength nephelometer, Aerosol Sci. Technol., 39, 17-29, 10.1080/027868290901972, 2005.

Backman, J., Virkkula, A., Vakkari, V., Beukes, J., Van Zyl, P., Josipovic, M., Piketh, S., Tiitta, P., Chiloane, K., Petäjä, T., Kulmala, M., and Laakso, L.: Differences in aerosol absorption Ångström exponents between correction algorithms for a particle soot absorption photometer measured on the South African Highveld, Atmos, Atmos. Meas. Tech., 7, 4285-4298, 10.5194/amt-7-4285-2014, 2014.

Backman, J., Schmeisser, L., Virkkula, A., Ogren, J. A., Asmi, E., Starkweather, S., Sharma, S., Eleftheriadis, K., Uttal, T., Jefferson, A., Bergin, M., Makshtas, A., Tunved, P., and Fiebig, M.: On Aethalometer measurement uncertainties and an instrument correction factor for the Arctic, Atmos. Meas. Tech., 10.5194/amt-10-5039-2017, 2017.

Bernardoni, V., Ferrero, L., Bolzacchini, E., Forello, A. C., Gregorič, A., Massabò, D., Močnik, G., Prati, P., Rigler, M., Santagostini, L., Soldan, F., Valentini, S., Valli, G., and Vecchi, R.: Determination of Aethalometer multiple-scattering enhancement parameters and impact on source apportionment during the winter 2017/18 EMEP/ACTRIS/COLOSSAL campaign in Milan, Atmos. Meas. Tech., 14, 2919-2940, 10.5194/amt-14-2919-2021, 2021.

Bond, T. C., Anderson, T. L., and Campbell, D.: Calibration and intercomparison of filter-based measurements of visible light absorption by aerosols, Aerosol Sci. Technol., 30, 582-600, 10.1080/027868299304435, 1999.

Bond, T. C., Covert, D. S., and Müller, T.: Truncation and angular-scattering corrections for absorbing aerosol in the TSI 3563 nephelometer, Aerosol Sci. Technol., 43, 866-871, 10.1080/02786820902998373, 2009.

Collaud Coen, M., Weingartner, E., Apituley, A., Ceburnis, D., Fierz-Schmidhauser, R., Flentje, H., Henzing, J., Jennings, S. G., Moerman, M., Petzold, A., Schmid, O., and Baltensperger, U.: Minimizing light absorption measurement artifacts of the Aethalometer: evaluation of five correction algorithms, Atmos. Meas. Tech., 3, 457-474, 10.5194/amt-3-457-2010, 2010.

Cuesta-Mosquera, A., Močnik, G., Drinovec, L., Müller, T., Pfeifer, S., Minguillón, M. C., Briel, B., Buckley, P., Dudoitis, V., Fernández-García, J., Fernández-Amado, M., Ferreira De Brito, J., Riffault, V., Flentje, H., Heffernan, E., Kalivitis, N., Kalogridis, A. C., Keernik, H., Marmureanu, L., Luoma, K., Marinoni, A., Pikridas, M., Schauer, G., Serfozo, N., Servomaa, H., Titos, G., Yus-Díez, J., Zioła, N., and Wiedensohler, A.: Intercomparison and characterization of 23 Aethalometers under laboratory and ambient air conditions: procedures and unit-to-unit variabilities, Atmos. Meas. Tech., 14, 3195-3216, 10.5194/amt-14-3195-2021, 2021.

Drinovec, L., Močnik, G., Zotter, P., Prévôt, A., Ruckstuhl, C., Coz, E., Rupakheti, M., Sciare, J., Müller, T., Wiedensohler, A., and Hansen, A. D. A.: The "dual-spot" Aethalometer: an improved measurement of aerosol black carbon with real-time loading compensation, Atmos. Meas. Tech., 8, 1965-1979, 10.5194/amt-8-1965-2015, 2015.

Drinovec, L., Gregorič, A., Zotter, P., Wolf, R., Bruns, E. A., Prévôt, A. S. H., Petit, J. E., Favez, O., Sciare, J., Arnold, I. J., Chakrabarty, R. K., Moosmüller, H., Filep, A., and Močnik, G.: The filter-loading effect by ambient aerosols in filter absorption photometers depends on the coating of the sampled particles, Atmos. Meas. Tech., 10, 1043-1059, 10.5194/amt-10-1043-2017, 2017.

Hari, P., and Kulmala, M.: Station for measuring ecosystem–atmosphere relations, Boreal Environ. Res., 10, 315-322, 2005.

Hari, P., Nikinmaa, E., Pohja, T., Siivola, E., Bäck, J., Vesala, T., and Kulmala, M.: Station for measuring ecosystem-atmosphere relations: SMEAR, in: Physical and Physiological Forest Ecology, Springer, 471-487, 2013.

Haywood, J., and Shine, K.: The effect of anthropogenic sulfate and soot aerosol on the clear sky planetary radiation budget, Geophys. Res. Lett., 22, 603-606, 10.1029/95GL00075, 1995.

Hyvärinen, A., Vakkari, V., Laakso, L., Hooda, R., Sharma, V., Panwar, T., Beukes, J., van Zyl, P., Josipovic, M., Garland, R. M., Andreae, M. O., Pöschl, U., and Petzold, A.: Correction for a measurement artifact of the Multi-Angle Absorption 483 Photometer (MAAP) at high black carbon mass concentration levels, Atmos. Meas. Tech., 6, 81-90, 10.5194/amt-6-81-2013, 2013.

Kanaya, Y., Taketani, F., Komazaki, Y., Liu, X., Kondo, Y., Sahu, L. K., Irie, H., and Takashima, H.: Comparison of Black Carbon Mass Concentrations Observed by Multi-Angle Absorption Photometer (MAAP) and Continuous Soot-Monitoring System (COSMOS) on Fukue Island and in Tokyo, Japan, Aerosol Sci. Technol., 47, 1-10, 10.1080/02786826.2012.716551, 2013.

Kebabian, P. L., Robinson, W. A., and Freedman, A.: Optical extinction monitor using cw cavity enhanced detection, Rev. Sci. Instrum., 78, 063102, 10.1063/1.2744223, 2007.

Kim, J.-H., Kim, S.-W., Ogren, J. A., Sheridan, P. J., Yoon, S.-C., Sharma, S., and Lin, N.-H.: Multiple scattering correction factor estimation for aethalometer aerosol absorption coefficient measurement, Aerosol Sci. Technol., 53, 160-171, 10.1080/02786826.2018.1555368, 2019.

Li, H., McMeeking, G. R., and May, A. A.: Development of a new correction algorithm applicable to any filter-based absorption photometer, Atmos. Meas. Tech., 13, 2865-2886, 10.5194/amt-13-2865-2020, 2020.

Lohmann, U., and Feichter, J.: Global indirect aerosol effects: A review, Atmos. Chem. Phys., 5, 715-737, 10.5194/acp-5-715-2005, 2005.

Luoma, K., Virkkula, A., Aalto, P., Petäjä, T., and Kulmala, M.: Over a 10-year record of aerosol optical properties at SMEAR II, Atmos. Chem. Phys., 19, 11363-11382, 10.5194/acp-19-11363-2019, 2019.

Massabò, D., Bernardoni, V., Bove, M. C., Brunengo, A., Cuccia, E., Piazzalunga, A., Prati, P., Valli, G., and Vecchi, R.: A multi-wavelength optical set-up for the characterization of carbonaceous particulate matter, J. Aerosol Sci, 60, 34-46, https://doi.org/10.1016/j.jaerosci.2013.02.006, 2013.

Miyakawa, T., Mordovskoi, P., and Kanaya, Y.: Evaluation of black carbon mass concentrations using a miniaturized aethalometer: Intercomparison with a continuous soot monitoring system (COSMOS) and a single-particle soot photometer (SP2), Aerosol Sci. Technol., 54, 811-825, 10.1080/02786826.2020.1724870, 2020.

Miyazaki, Y., Kondo, Y., Sahu, L. K., Imaru, J., Fukushima, N., and Kano, M.: Performance of a newly designed continuous soot monitoring system (COSMOS), J. Environ. Monit., 10, 1195-1201, 10.1039/B806957C, 2008.

Moteki, N., Kondo, Y., Nakayama, T., Kita, K., Sahu, L. K., Ishigai, T., Kinase, T., and Matsumi, Y.: Radiative transfer modeling of filter-based measurements of light absorption by particles: Importance of particle size dependent penetration depth, J. Aerosol Sci, 41, 401-412, 10.1016/j.jaerosci.2010.02.002, 2010.

Müller, T., Henzing, J., De Leeuw, G., Wiedensohler, A., Alastuey, A., Angelov, H., Bizjak, M., Coen, M., Engstrom, J., Gruening, C., Hillamo, R., Hoffer, A., Imre, K., Ivanow, P., Jennings, G., Sun, J., Kalivitis, N., Karlsson, H., Komppula, M., Laj, P., Li, S.-M., Lunder, C., Marinoni, A., Martins dos Santos, S., Moerman, M., Nowak, A., Ogren, J., Petzold, A., Pichon, J., Rodriquez, S., Sharma, S., Sheridan, P., Teinilä, K., Tuch, T., Viana, M., Virkkula, A., Weingartner, E., Wilhelm, R., and Wang, Y.: Characterization and intercomparison of aerosol absorption photometers: result of two intercomparison workshops, Atmos. Meas. Tech., 4, 245-268, 10.5194/amt-4-245-2011, 2011a.

Müller, T., Laborde, M., Kassell, G., and Wiedensohler, A.: Design and performance of a three-wavelength LED-based total scatter and backscatter integrating nephelometer, Atmos. Meas. Tech., 4, 1291-1303, 10.5194/amt-4-1291-2011, 2011b.

Müller, T., Virkkula, A., and Ogren, J. A.: Constrained two-stream algorithm for calculating aerosol light absorption coefficient from the Particle Soot Absorption Photometer, Atmos. Meas. Tech., 7, 4049-4070, 10.5194/amt-7-4049-2014, 2014.

Ogren, J. A.: Comment on "Calibration and intercomparison of filter-based measurements of visible light absorption by aerosols", Aerosol Sci. Technol., 44, 589-591, 10.1080/02786826.2010.482111, 2010.

Ogren, J. A., Wendell, J., Andrews, E., and Sheridan, P. J.: Continuous light absorption photometer for long-term studies, Atmos. Meas. Tech., 10, 4805-4818, 10.5194/amt-10-4805-2017, 2017.

Park, S. S., Hansen, A. D. A., and Cho, S. Y.: Measurement of real time black carbon for investigating spot loading effects of Aethalometer data, Atmos. Environ., 44, 1449-1455, https://doi.org/10.1016/j.atmosenv.2010.01.025, 2010.

Petzold, A., and Schönlinner, M.: Multi-angle absorption photometry—a new method for the measurement of aerosol light absorption and atmospheric black carbon, J. Aerosol Sci, 35, 421-441, 10.1016/j.jaerosci.2003.09.005, 2004.

Sandradewi, J., Prévôt, A. S., Szidat, S., Perron, N., Alfarra, M. R., Lanz, V. A., Weingartner, E., and Baltensperger, U.: Using aerosol light absorption measurements for the quantitative determination of wood burning and traffic emission contributions to particulate matter, Environ. Sci. Technol., 42, 3316-3323, 10.1021/es702253m, 2008.

Saturno, J., Pöhlker, C., Massabò, D., Brito, J., Carbone, S., Cheng, Y., Chi, X., Ditas, F., Hrabě de Angelis, I., Morán-Zuloaga, D., Pöhlker, M. L., Rizzo, L. V., Walter, D., Wang, Q., Artaxo, P., Prati, P., and Andreae, M. O.: Comparison of different Aethalometer correction schemes and a reference multi-wavelength absorption technique for ambient aerosol data, Atmos. Meas. Tech., 10, 2837-2850, 10.5194/amt-10-2837-2017, 2017.

Schmid, O., Artaxo, P., Arnott, W. P., Chand, D., Gatti, L. V., Frank, G. P., Hoffer, A., Schnaiter, M., and Andreae, M. O.: Spectral light absorption by ambient aerosols influenced by biomass burning in the Amazon Basin. I: Comparison and field calibration of absorption measurement techniques, Atmos. Chem. Phys., 6, 3443-3462, 10.5194/acp-6-3443-2006, 2006.

Segura, S., Estellés, V., Titos, G., Lyamani, H., Utrillas, M. P., Zotter, P., Prévôt, A. S. H., Močnik, G., Alados-Arboledas, L., and Martínez-Lozano, J. A.: Determination and analysis of in situ spectral aerosol optical properties by a multi-instrumental approach, Atmos. Meas. Tech., 7, 2373-2387, 10.5194/amt-7-2373-2014, 2014.

Shen, Y., Virkkula, A., Ding, A., Wang, J., Chi, X., Nie, W., Qi, X., Huang, X., Liu, Q., Zheng, L., Zheng, X., Petäjä, T., Aalto, P., Fu, C., and Kulmala, M.: Aerosol optical properties at SORPES in Nanjing, east China, Atmos. Chem. Phys., 18, 5265-5292, 10.5194/acp-18-5265-2018, 2018.

Sherman, J., Sheridan, P., Ogren, J., Andrews, E., Hageman, D., Schmeisser, L., Jefferson, A., and Sharma, S.: A multi-year study of lower tropospheric aerosol variability and systematic relationships from four North American regions, Atmos. Chem. Phys., 15, 12487-12517, 10.5194/acp-15-12487-2015, 2015.

Song, S., Wu, Y., Xu, J., Ohara, T., Hasegawa, S., Li, J., Yang, L., and Hao, J.: Black carbon at a roadside site in Beijing: Temporal variations and relationships with carbon monoxide and particle number size distribution, Atmos. Environ., 77, 213-221, 10.1016/j.atmosenv.2013.04.055, 2013.

Stocker, T. F., Qin, D., Plattner, G.-K., Tignor, M., Allen, S. K., Boschung, J., Nauels, A., Xia, Y., Bex, V., and Midgley, P. M.: Climate change 2013: The physical science basis, 2013.

Svensson, J., Ström, J., and Virkkula, A.: Multiple-scattering correction factor of quartz filters and the effect of filtering particles mixed in water: implications for analyses of light absorption in snow samples, Atmos. Meas. Tech., 12, 5913-5925, 10.5194/amt-12-5913-2019, 2019.

Wang, Y., Hopke, P. K., Rattigan, O. V., Xia, X., Chalupa, D. C., and Utell, M. J.: Characterization of residential wood combustion particles using the two-wavelength aethalometer, Environ. Sci. Technol., 45, 7387-7393, 10.1021/es2013984, 2011.

Weingartner, E., Saathoff, H., Schnaiter, M., Streit, N., Bitnar, B., and Baltensperger, U.: Absorption of light by soot particles: determination of the absorption coefficient by means of Aethalometers, J. Aerosol Sci, 34, 1445-1463, 10.1016/S0021-8502(03)00359-8, 2003.

Virkkula, A., Ahlquist, N. C., Covert, D. S., Arnott, W. P., Sheridan, P. J., Quinn, P. K., and Coffman, D. J.: Modification, calibration and a field test of an instrument for measuring light absorption by particles, Aerosol Sci. Technol., 39, 68-83, 10.1080/027868290901963, 2005.

Virkkula, A., Mäkelä, T., Hillamo, R., Yli-Tuomi, T., Hirsikko, A., Hämeri, K., and Koponen, I. K.: A simple procedure for correcting loading effects of Aethalometer data, J. Air Waste Ma., 57, 1214-1222, 10.3155/1047-3289.57.10.1214, 2007.

Virkkula, A.: Correction of the calibration of the 3-wavelength particle soot absorption photometer (3λ PSAP), Aerosol Sci. Technol., 44, 706-712, 10.1080/02786826.2010.482110, 2010.

Virkkula, A., Backman, J., Aalto, P., Hulkkonen, M., Riuttanen, L., Nieminen, T., Dal Maso, M., Sogacheva, L., De Leeuw, G., and Kulmala, M.: Seasonal cycle, size dependencies, and source analyses of aerosol optical properties at the SMEAR II measurement station in Hyytiala, Finland, Atmos. Chem. Phys., 11, 4445–4468, 10.5194/acp-11-4445-2011, 2011.

Virkkula, A., Chi, X., Ding, A., Shen, Y., Nie, W., Qi, X., Zheng, L., Huang, X., Xie, Y., Wang, J., Petäjä, T., and Kulmala, M.: On the interpretation of the loading correction of the Aethalometer, Atmos. Meas. Tech., 8, 4415-4427, 10.5194/amt-8-4415-2015, 2015.

WMO/GAW: Aerosol measurement procedures, guidelines and recommendations, 2nd edition, GAW Report No. 227, World Meteorological Organization, Geneva, Switzerland, 2016.

Zotter, P., Herich, H., Gysel, M., El-Haddad, I., Zhang, Y., Močnik, G., Hüglin, C., Baltensperger, U., Szidat, S., and Prévôt, A. S.: Evaluation of the absorption Ångström exponents for traffic and wood burning in the Aethalometer-based source apportionment using radiocarbon measurements of ambient aerosol, Atmos. Chem. Phys., 17, 4229-4249, 10.5194/acp-17-4229-2017, 2017.

Table 1. All the wavelength dependent coefficients used in the AE31 correction algorithms proposed by Weingartner et al. (2003) and Arnott et al. (2005). TAlso, the extrapolated values of the multiple scattering correction factor used in the Arnott et al. (2005) correction algorithm (C_{ARN}) at different wavelengths are presented in the table.

Coefficients for AE31 correction algorithm by Weingartner et al. (2003)							
λ (nm)	370	470	520	590	660	880	950
a	0.88878	0.87868	0.863	0.86857	0.850	0.83829	0.822
ω	0.91	0.89	0.89	0.88	0.85	0.83	0.82
f	1.0798	1.09610	1.10095	1.1031	1.128	1.141	1.1485
Coefficients for AE31 correction algorithm by Arnott et al. (2005)							
λ (nm)	370	470	520	590	660	880	950
$100 \cdot a_{s.ARN}$	3.35	4.57	5.23	6.16	7.13	10.38	11.48
$\tau_{a,fx}$	0.3026	0.2527	0.2338	0.2129	0.1956	0.1575	0.1486
C_{ARN}	2.70	2.82	2.87	2.94	3.00	3.16	3.20

Table 122. Average values for the multiple scattering correction factor (C_{ref}) for the different correction algorithms. These values are reported at the Aethalometer wavelength 637 nm. The slope of the fit, and the standard error of the fit (SE), and 95 % confidence interval (CI) were determined by a linear regression applied for the whole data set. The median, mean, and standard deviation (SD), as well as the 5th and 95th percentile range were determined from the C_{ref} values that were calculated for each data point separately.

	fit	SE	95 % CI	median	mean	SD	5th & 95th percentiles
C_{WEI}	3.00	0.003	[2.99; 3.00]	3.34	3.29	0.57	[2.59; 4.26]
C_{ARN}				3.13	3.13	0.45	[2.49; 3.81]
C_{VIR}	3.14	0.002	[3.13; 3.14]	3.30	3.28	0.56	[2.53; 4.18]
C_{COL}	2.99	0.003	[2.98; 2.99]	3.28	3.32	0.57	[2.55; 4.23]
C_{NC}	2.77	0.003	[2.76; 2.77]	3.09	3.06	0.55	[2.32; 3.95]

Table 3. Linear fits between the AE31 vs. reference absorption ($\sigma_{abs,ref}$ measured by MAAP) for different *ATN* intervals (at 660 nm) as well as between the PSAP vs. $\sigma_{abs,ref}$. The value in parenthesis is the coefficient of determination (R^2).

ATN	0 - 20	20 - 40	40 - 60	60 - 80
W2003	1.05·x + 0.07 (0.98)	0.99·x + 0.15 (0.97)	0.95·x + 0.15 (0.96)	0.97·x + 0.12 (0.94)
A2005	0.93·x + 0.06	0.93·x + 0.16	0.97·x + 0.15	1.06·x + 0.10

	(0.96)	(0.95)	(0.92)	(0.90)
V2007	1.02·x + 0.05 (0.98)	0.98·x + 0.10 (0.98)	0.97·x + 0.08 (0.97)	0.99·x + 0.05 (0.96)
CC2010	1.01·x + 0.06 (0.98)	0.95·x + 0.15 (0.97)	0.92·x + 0.16 (0.95)	0.95·x + 0.13 (0.92)
Not corrected	1.12·x + 0.07 (0.98)	1.01·x + 0.15 (0.97)	0.93·x + 0.14 (0.96)	0.93·x + 0.12 (0.95)
Tr	**1 – 0.7**	**1 – 0.4**	**0.4 – 0.7**	**0 – 0.4**
B1999	1.04·x + 0.01 (0.97)	1.06·x + 0.02 (0.97)	1.06·x + 0.07 (0.97)	1.11·x + 0.02 (0.98)
V2010	1.01·x - 0.02 (0.96)	1.12·x - 0.07 (0.94)	1.17·x + 0.01 (0.95)	1.46·x - 0.20 (0.96)

Table 44. The mean compensation parameters (*k*) and the wavelength dependency of ~~the~~ *k* (a_k) for the AE31 correction algorithm suggested by Virkkula et al. (2007). The average values are calculated over all the seasons, but also separately for each season. The seasons were classified as: spring (March – May), summer (June – August), autumn (September – November), and winter (December – February).

Season	370 nm ($\cdot 10^{-3}$)	470 nm ($\cdot 10^{-3}$)	520 nm ($\cdot 10^{-3}$)	590 nm ($\cdot 10^{-3}$)	660 nm ($\cdot 10^{-3}$)	880 nm ($\cdot 10^{-3}$)	950 nm ($\cdot 10^{-3}$)	a_k ($\cdot 10^{-6}$ nm^{-1})
all	4.6 ± 7.0	3.6 ± 7.2	3.5 ± 8.0	3.4 ± 8.9	2.7 ± 9.5	2.1 ± 10.6	2.0 ± 10.8	-4.2
spring	4.4 ± 7.0	3.5 ± 6.5	3.4 ± 7.6	3.4 ± 8.8	2.8 ± 9.2	2.2 ± 10.5	2.2 ± 10.2	-3.5
summer	3.0 ± 6.7	1.5 ± 6.3	1.1 ± 6.9	0.5 ± 9.0	-0.4 ± 9.6	-1.7 ± 10.3	-2.5 ± 11.3	-8.8
autumn	4.6 ± 7.7	3.6 ± 9.1	3.6 ± 9.7	3.5 ±10.3	2.8 ±10.2	2.5 ± 10.9	2.2 ± 12.1	-3.6
winter	5.5 ± 6.3	4.8 ± 6.4	4.8 ± 7.0	4.8 ± 6.9	4.3 ± 8.4	4.4 ± 9.9	4.3 ± 9.1	-1.7

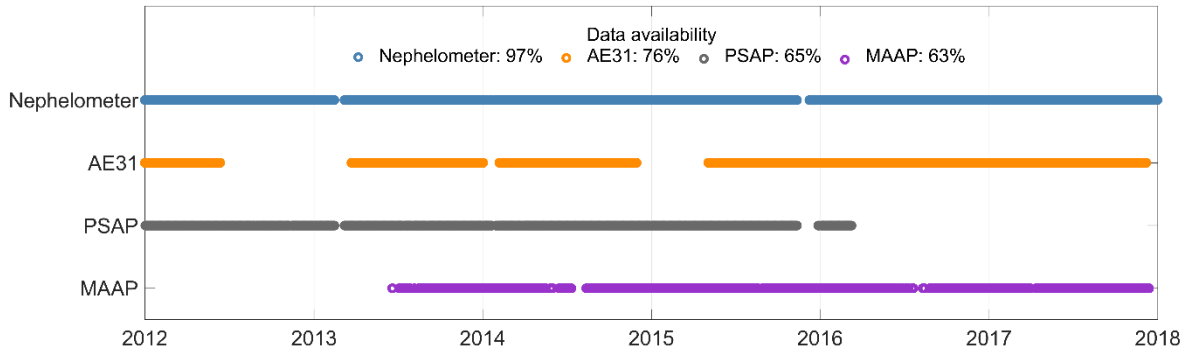

~~**Figure 1: The availability of the optical aerosol data at SMEAR II station from the integrating nephelometer, AE31, PSAP, and MAAP. The dots represent days that had at least 50% of data available. The data availability for each instrument for the whole period of 2012 – 2017 is given in the legend.**~~

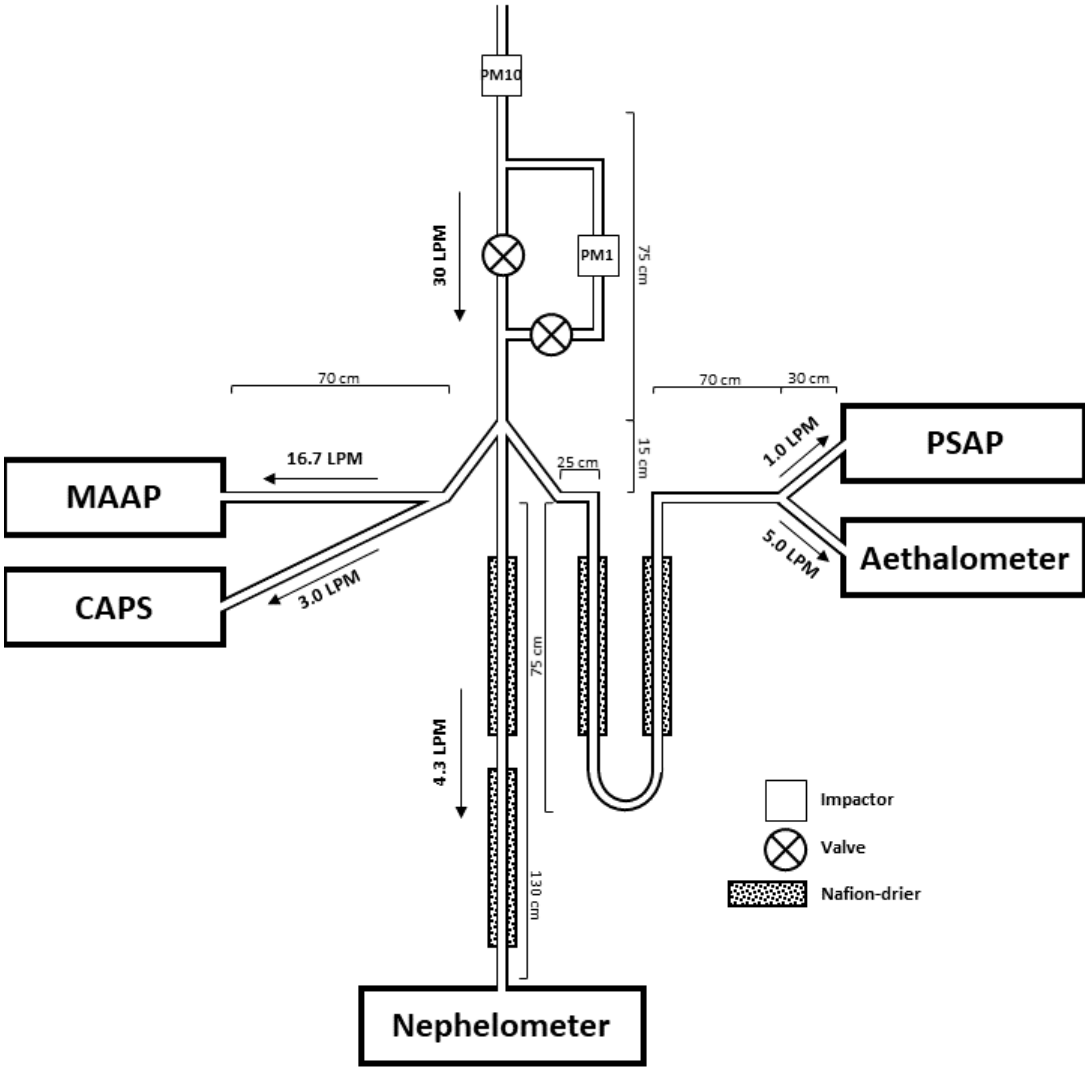

Figure ~~2~~1: Measurement scheme for the instruments that measured the aerosol optical properties at the SMEAR II station. This setup was running during 2014–2015, when all the instruments were operating in parallel.

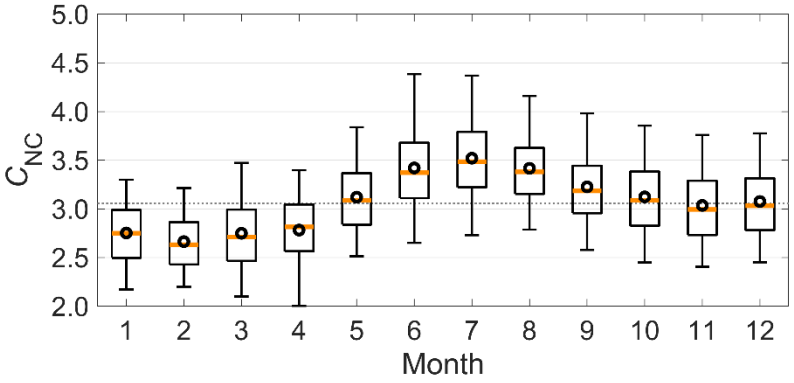

Figure ~~3~~2. The seasonal variation ~~of~~ in the multiple scattering correction factor for not corrected data (C_{NC}). The orange line in the middle of the box is the median, the black circle is the mean, the edges of the boxes represent the 25th and 75th percentiles, and the whiskers represent the 10th and 90th percentiles of the data. The dashed line is the median for all data~~median C_{NC} is presented with a dashed line.~~

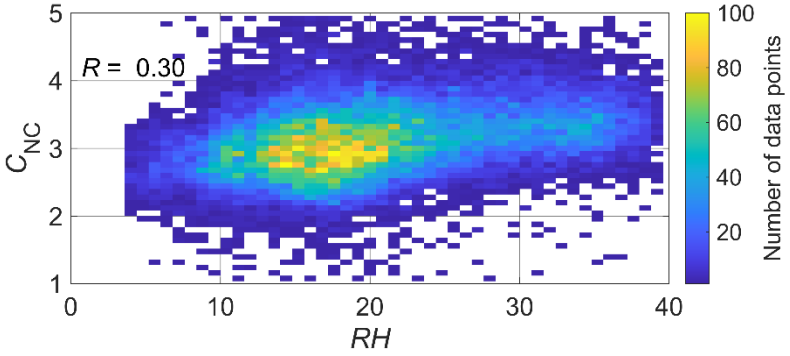

Figure ~~3~~4. The dependency of the multiple scattering correction factor for not corrected data (C_{NC}) on the instrumental relative humidity (RH) in the MAAP. The colored grid points represent the number of data points in each grid point. There is 50 grid points in x- and y-directions so in total there are 2500 grid points.

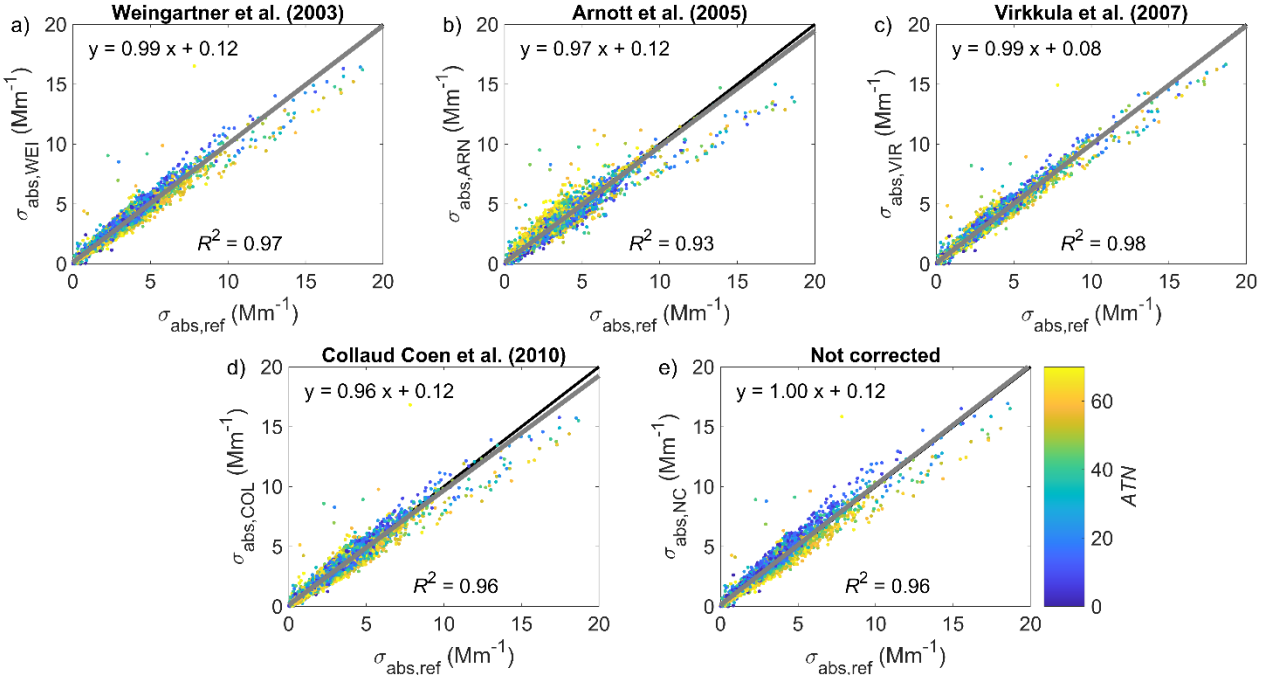

Figure 45. Comparison of the AE31 and MAAP measurements for all the different AE31 correction algorithms. The corrected AE31 data has been interpolated to the same wavelength with MAAP (637 nm). The data points are colored by the AE31 filter attenuation (*ATN*; at 660 nm). The fit to the data is presented with a grey line and the equation and the ~~correlation~~ coefficient of determination (R^2) are shown in the subfigures. One-to-one line is shown with black color.

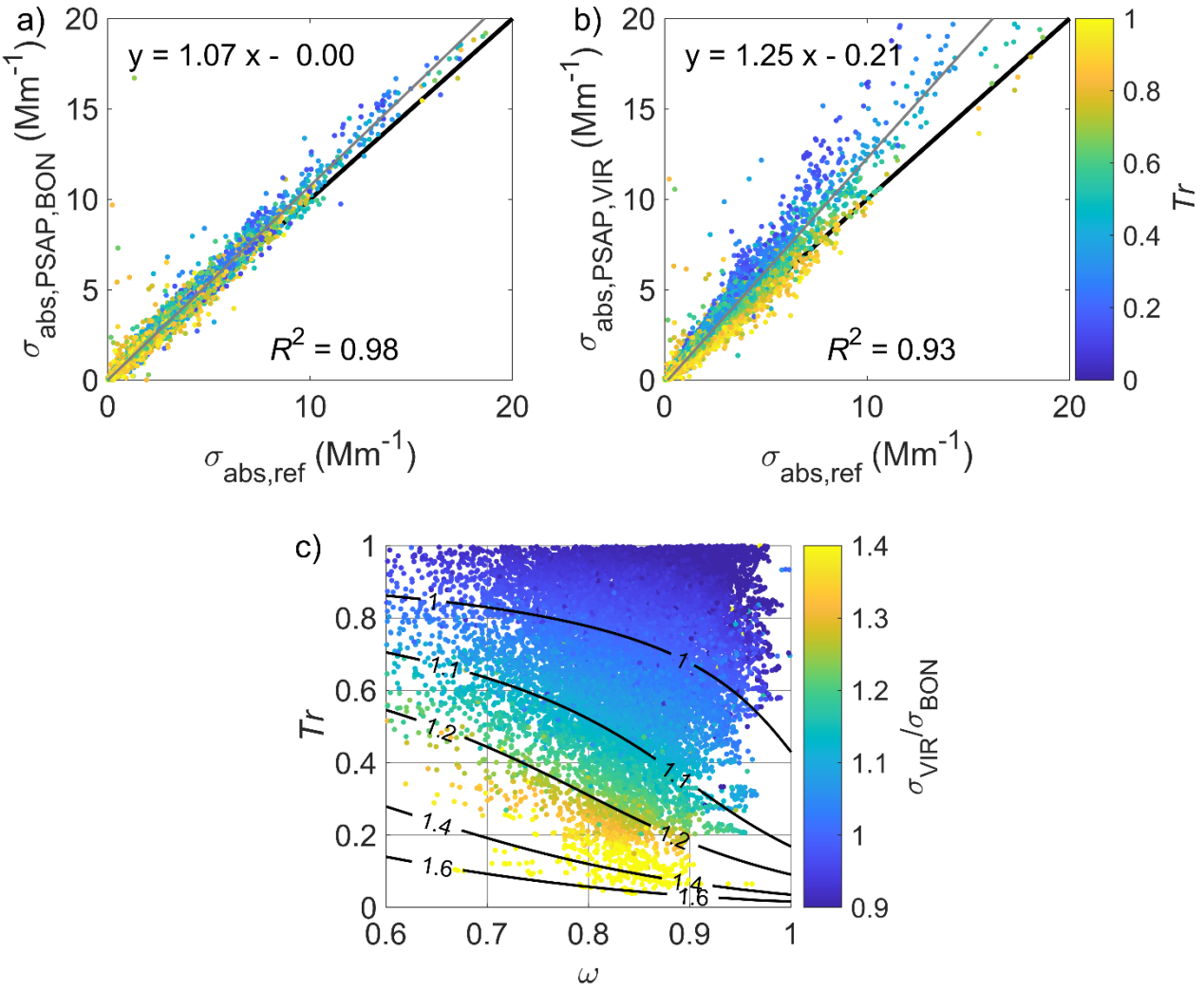

Figure 5~~6~~. The a) and b) subfigures present the comparison of the PSAP and MAAP measurements for both B1999 and V2010 correction algorithms, respectively. The data points are colored b~~e~~y the PSAP filter transmittance (*Tr*), the fit to the data is presented with a grey line, and the equation and the ~~correlation~~ coefficient of determination (R^2) are shown in the subfigures. One-to-one line is shown with black color. The subfigure c) presents the relation of the PSAP derived absorption coefficients corrected with the V2010 algorithm ($\sigma_{abs,PSAP,VIR}$) and the B1999 algorithm depends on the *Tr* and single scattering albedo (ω). The contour lines show the theoretically determined $\sigma_{abs,PSAP,VIR}/\sigma_{abs,PSAP,BON}$ ratio. The ω was determined from nephelometer and MAAP measurements at 637 nm.

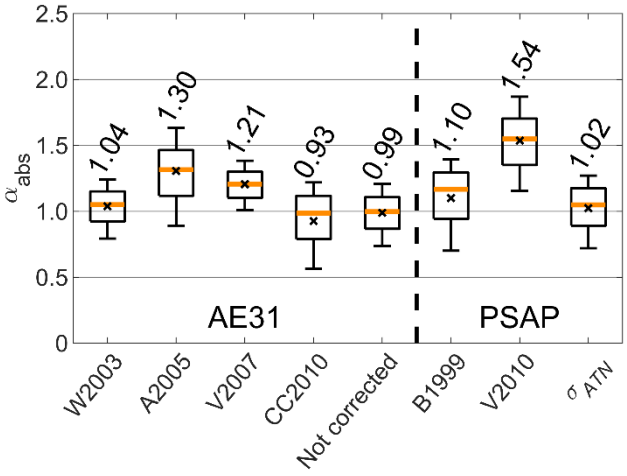

Figure 6~~7~~. The absorption Ångström exponent (α_{abs}) for all the different AE31 and PSAP correction algorithms. The orange line in the middle of the box is the median, the black circle is the mean, the edges of the boxes represent the 25th and 75th percentiles, and the whiskers represent the 10th and 90th percentiles of the data. ~~The explanation for the boxplots is the same as in Fig. 5.~~The values given above each box show the according median values.

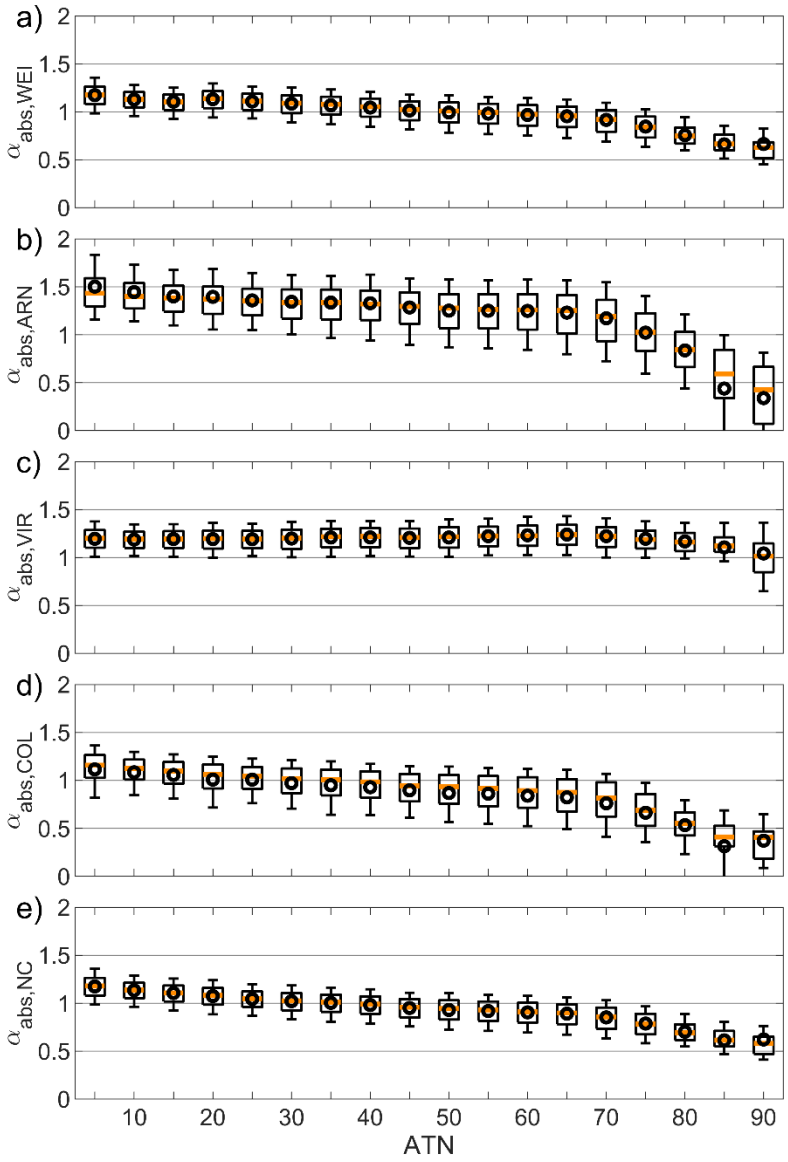

Figure 8. The dependency of the absorption Ångström exponent (α_{abs}) on the AE31 filter attenuation (*ATN*; at 660 nm) for different correction algorithms. The orange line in the middle of the box is the monthly median, the black circle is the mean, the edges of the boxes represent the 25th and 75th percentiles, and the whiskers represent the 10th and 90th percentiles of the data. ~~The explanation for the boxplots is the same as in Fig. 5.~~

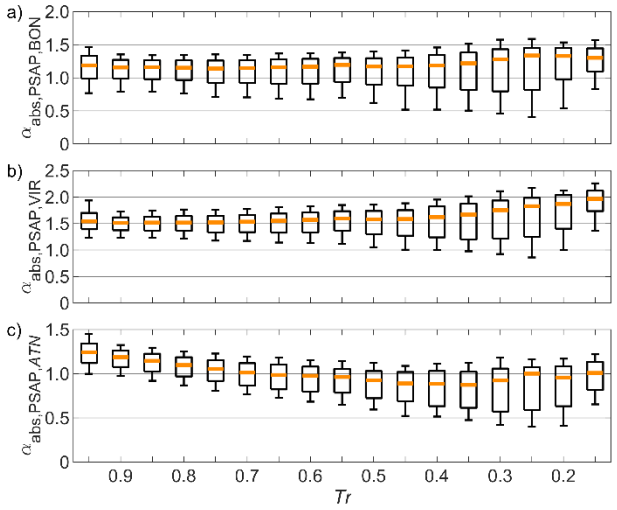

Figure 89. The dependency of the absorption Ångström exponent (α_{abs}) on the PSAP filter transmittance (*Tr*) for the a) B1999, b) V2010, and c) not corrected σ_{ATN}. The explanation for the boxplots is the same as in Fig. 5.

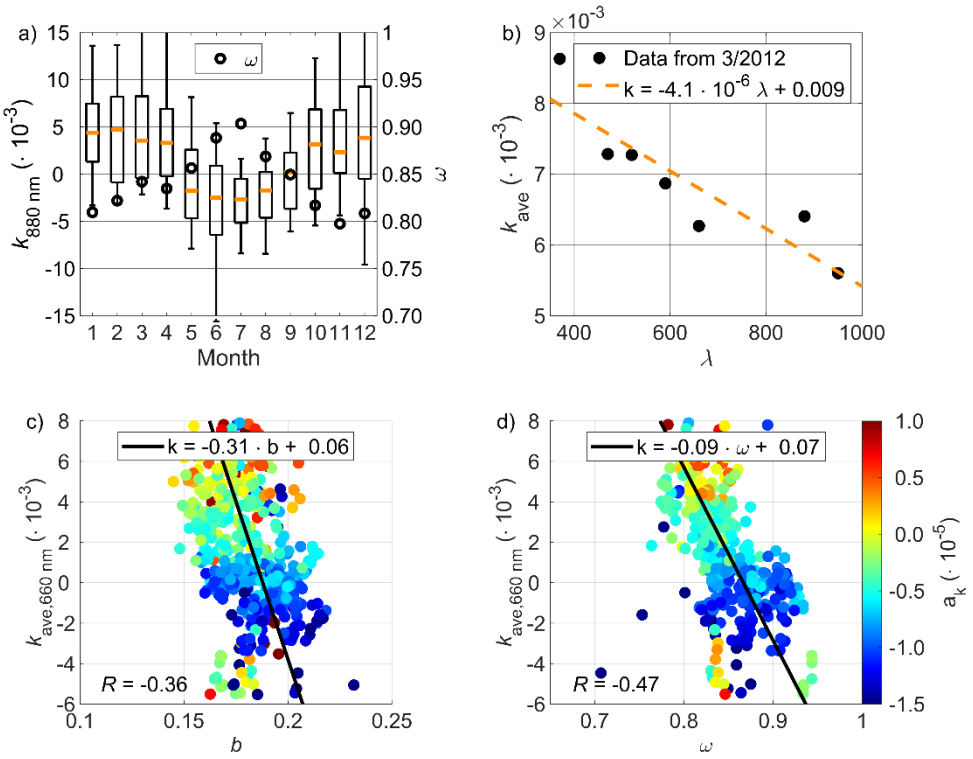

Figure 9~~10~~. a) The seasonal variation ~~of~~ in the compensation parameter (*k*). b) An example of calculating the wavelength dependency of the *k* (a_k). c) The dependency of the *k* on the backscatter fraction (*b*). The data points are coloured by a_k. d) The dependency of the *k* on the single scattering albedo (ω). The data points are coloured by a_k.